Chapter 5
Chlorosulfonated Rubber-Based Nanoblends: Preparation, Characterization and Applications

Gordana Marković, Milena Marinović-Cincović, Vojislav Jovanović, Suzana Samaržija-Jovanović and Jaroslava Budinski-Simendić

Abstract In this chapter, the preparation, characterization, and applications of chlorosulphonated polyethylene (CSM) rubber based nano blends have been investigated. CSM rubber based nanoblend compounds have been prepared on a laboratory-size (300x600 mm) two-roll mixing mill maintained at 40 ± 5 °C. Curing was performed at 160 °C up to the optimum cure time (t), which was determined from the rheograph using a Monsanto R-100 model. The mechanical properties, namely tensile strength (TS), tensile modulus at 100 % and 300 % elongation (M100 and M300), elongation at break (Eb%) and hardness have been followed up as a function of nano fillers and irradiation dose (dose rate of 10 kGy h^{-1} and total absorbed dose of 100, 200, 300, and 400 kGy) as well as blend composition. Cross-linking density has been determined using swelling measurements. A scanning electron microscope has been used for morphological study. Thermal stability of samples has been determined using thermogravimetric (TG) measurements. Dynamical mechanical properties were studied on a mechanical analyzer. The assignment of the principal bands in chlorosulphonated polyethylene (CSM) rubber based nano blends has been carried out by FTIR ATR spectra. Elastomeric materials based on the chlorosulfonated polyethylene (CSM) rubber nanoblend have a quite good crack resistance, wet grip, and weather resistance. On the other hand, they show a good resistance to interactions with alcohol's as well as strong acids and bases. This type of material also exhibits excellent ultraviolet light and oxygen stability.

G. Marković (✉)
Tigar, Nikole Pašića 213, 18300 Pirot, Serbia
e-mail: gordana1markovic@gmail.com

M. Marinović-Cincović
Institute of Nuclear Science Vinča, University of Belgrade, Belgrade, Serbia

V. Jovanović · S. Samaržija-Jovanović
Faculty of Natural Science and Mathematics, University of Priština,
Kosovska Mitrovica, Serbia

J. Budinski-Simendić
Faculty of Technology, University of Novi Sad, Novi Sad, Serbia

5.1   Introduction

Blends of rubbers are of technological and commercial importance, since they allow
the user to access properties of the final blended and vulcanized rubber that is not
accessible from a single, commercially available rubber alone. These potentially
improved properties include chemical, physical, and processing benefits. In reality,
all blends show compositionally correlated changes in all of these properties com-
pared to the blend components. The technology of rubber blends is largely focused
on the choice of individual rubbers and the creation of the blends to achieve a set of
final properties [1]. Miscible blends of rubbers that consist of a single rubber phase
with microscopically uniform cross-linking and distribution of reinforcing agents
reflect a compositionally weighted average of the microscopic properties of the
constituents. Miscible blends are commonly used though they have been very rarely
recognized. Analysis of such blends, particularly after vulcanization, is difficult. The
current analytical techniques are only slightly more capable than the classical
techniques of selective precipitation of the components of an unvulcanized rubber
blend from solution [2]. Immiscible blends show additional, more complex changes
due to a microscopically inhomogeneous phase structure of the two component
rubbers. The two separate phases typically have differences in the retention of the
fillers and plasticizers as well as vulcanization in the presence of the curative.
Changing the properties of rubbers by uneven distribution of fillers and vulcaniza-
tion is, however, the more common use of blends of immiscible rubbers [3].

Many reviews [4–6] are focused on immiscible blends of rubbers. Isobutylene-
based rubbers include butyl rubber and halogenated butyl rubber, and due to their
impermeability and resistance to heat and oxidation, these polymers find application
in tire innerliners, innertubes, curing bladders and envelopes, and other specialty
applications where air retention and resistance to heat and oxidation are desired [7].
Chlorosulfonated polyethylene (CSM) is an important rubber which has been fre-
quently used in many applications such as sheeting cable and geomembrane due to
its outstanding resistance to deterioration by heat, oils, ozone, and oxidation [8].
The blending together of isobutylene-based rubbers (IIR) with chlorosulfonated
polyethylene (CSM) is intended to produce a vulcanizate with the best properties
from each component, i.e., CSM's impermeability and IIR and CIIR's good
strength properties and resistance to oil [9]. Chlorobutyl (CIIR) and bromobutyl
(BIIR) rubbers are manufactured similarly to butyl rubber, but with an added
subsequent halogenation step. Due to the nearly equivalent reactivity ratios of the
monomers and low concentration of isoprene, the isoprenyl units in these polymers
are randomly distributed along the polymer chain. Commercially, chlorobutyl
rubber (CIIR) and bromobutyl rubber (BIIR) are the most important derivatives of
butyl rubber. Their predominant application is in tire innerliners with the

performance of the modern radial tire being impacted by the amount of halobutyl rubber used in the innerliner compound. Typical performance requirements of the tire innerliner are air retention, adhesion to tire carcass compound, resistance to fatigue and cracking, heat resistance, high tensile, and tear strength [10].

Silica has been used as non-black reinforcing filler in the rubber industry for a long time. Reinforced rubber blends are suitable materials for industrial practice [11]. Obviously, in such systems, both components (filler and rubber) have the reactive groups for the additional cross-linking reaction to take place [12]. Besides the so-called dispersion forces, there are a variety of other interactions between particles. A key one among them is hydrogen bonding, which tends to be a significant force in the case of fumed silica, where hydrogen bonding between surface silanol groups takes place. Many authors have investigated the role of filler networking in the elastic properties of elastomer composites [13]. The surface of hydrated or precipitated silica is highly polar and hydrophilic because of the presence of numerous silanol groups. The evaluation of the reinforcing effect is usually based on the determination of the processability of elastomers and the dynamic mechanical properties of cross-linked materials [14].

Among many other particulate fillers, the use of carbon black (CB) is very important in rubber technology for obtaining elastomers with good dynamic mechanical as well as ultimate properties. New materials are also considered as fillers, whether for more economical reasons or rather to impart some desirable characteristics [15, 16] of CB as one of the major inputs in tire industry, has some extraordinary features. The surface specific area of CB is considered to be one of the most critical parameters considered for achieving a high degree of reinforcement. This characteristic property supplies the necessary adsorption sites to the polymer chains for wetting. As polymer chains may also enter into the voids of the filler agglomerates and aggregates, the rheological properties (especially the viscosity) of the filled polymer melts are affected by both the so-called physical entrapment and the physical cross-links, created by a strong physisorption of the chains on the filler surface. These effects may also play an important role in the reinforcement of cross-linked elastomeric matrices. One of the most important parameters for the performance of a composite material is the degree of adhesion (phase bonding) at the matrix–filler interface [17]. In this study, fourteen different SBR/CSM formulations were produced by mechanical mixing and vulcanized. The mechanical properties such as the hardness, the modulus, the tensile strength, and the abrasion loss were investigated. On the other hand, some physical characteristics were investigated via the vulcanization test.

The main interest was related to the effect of biogenic silica (BSi) as a filler on the deformation mechanisms and mechanical properties of composites based on the polymer matrix. Diatomaceous comes as a biogenic silica (BSi) from the word diatom, which is the single-celled aquatic plant. Diatoms are living phytoplanktons which form an important part of marine and freshwater. The silicate shell, termed "frustule," supports a fleshy body. The fossil beds are skeletons sunk to the bed of lake or sea after the body died and formed deposits there. Diatoms are found in a great variety of forms [18]. The skeletal remains of diatoms with submicron-sized

hole are described as "indescribable particle shape" far from any simple classification [19]. The specific diatom morphology and chemical resistance could be the base of using this material as filler in composites. There is little in the literature on this subject. Adhesion between matrix and filler phases in composites is important in crack propagation and composite failure. The study of the deformation and failure process, their relation to the structure of composite, and the strength of interactions between the polymer matrix and filler phases may provide useful information for the development of the new composite materials with diatoms.

5.2 Preparation

The rubber-based nano-blend compounds were prepared using a laboratory mixing roll mill of dimensions 400×150 mm at a speed ratio of the rollers $n_1/n_2 = 28/22$, at a roller temperature of 40–50 °C. The time of the preparation of the blends was ca. 20 min. Curing was performed at 160 °C up to the optimum cure time (t_{c90}), which was determined from the rheograph obtained using a Monsanto R-100 model. The addition of ingredients during mixing was carried following the same order and conditions of mixing. Two different types of rubbers were used IIR and CIIR blended with CSM at different ratios. IIR (Butyl 068), Mooney viscosity 51 (ML1+8 at 125 °C) with isoprene content of 1.15 mol% and CIIR (Chlorobutyl 1066), Mooney viscosity 38 (ML1+8 at 125 °C) with isoprene content of 1.95 mol % and halogen content of 1.26 mol% were supplied by Exxon Mobil, England. Their respective technical specifications are shown in Tables 5.1 and 5.2, and the compound formulations of the samples are given in Tables 5.3, 5.4, 5.5, and 5.6.

The compound formulation is given in Table 5.4.

Table 5.1 Analytical data for the fillers

Filler	BET $(N_2)/m^2g^{-1}$	DBP absorption/cm^3 100 g^{-1}	pH	Particle size
Nano-silica	160–200	220	6.7	15 nm
Micro-silica	/	130	10	28 μm

Table 5.2 Technical specification of isobutylene-co-isoprene (IIR), chlorinated isobutylene-co-isoprene, and chlorosulfonated polyethylene (CSM) rubbers

Elastomer	Grade	Mooney viscosity (ML1 +8 at 125 °C)	Isoprene (mol%)/sulfur content (mol%)	Halogen (mol%)	Halogen (mol%)
Isobutylene-co-isoprene (IIR) rubber	Butyl 068	51	1.15	–	–
Chlorinated isobutylene-co-isoprene rubber	Chlorobutyl 1068	38	1.95	Cl	1.28
Chlorosulfonated polyethylene (CSM) rubber	Hypalon 40S	46	1	Cl	34.5

5.3   Characterization

5.3.1   Cure Characteristics

The sheeted rubber compound was conditioned at 23 ± 2 °C for 24 h prior to cure assessment on a Monsanto moving die rheometer (model 100S, USA) at 160 °C. The compound formulations (Tables 5.3, 5.4, 5.5, and 5.6) are expressed in part per hundred parts of rubber (phr). All test specimens were compression-molded at 160 °C during the respective optimum cure time (t_{c90}) determined from the Monsanto rheometer. The scorch time, t_{s2}, is the time to 2 units of torque increase above minimum torque, and optimum cure time, t_{c90}, is the time to 90 % of maximum torque development calculated from the following expression:

$$M_{t90} = (M_h - M_l) \times 0.9 + M_l \qquad (5.1)$$

where M_h is the maximum torque and M_{c90} is a optimum cure time determined from the cure traces generated at 160 ± 2 °C by oscillating disk rheometer curemeter at

Table 5.3 Formulation of the compounds and nano- and micro-silica particle-sized filled polychloroprene (CR) and chlorosulfonated polyethylene rubber blends

Compounds (phr[a])	1	2	3	4	5	6	7
CSM	50	50	50	50	50	50	50
CR	50	50	50	50	50	50	50
ZnO	2.5	2.5	2.5	2.5	2.5	2.5	2.5
Stearic acid	2	2	2	2	2	2	2
Nano-silica	0	10	20	35	0	0	0
Micro-silica	0	0	0	0	10	20	35
Naphthenic oil	0	3.3	6.7	10	3.3	6.7	10
MgO	2	2	2	2	2	2	2
ETU	0.5	0.5	0.5	0.5	0.5	0.5	0.5
TMTD	1	1	1	1	1	1	1
S	0.5	0.5	0.5	0.5	0.5	0.5	0.5
Diethylene glycol	0	0.3	0.6	1.1	0.3	0.6	1.1

[a]Part per hundred parts of rubber

Table 5.4 Blend formulations (phr) of IIR and CIIR with CSM (cure system: 5.0 phr zinc oxide, 2.0 phr stearic acid, 0.5 phr MBTS, 2 phr TMTD, and 2 phr sulfur)

CSM	IIR/CIIR
100	0
80	20
60	40
40	60
20	80
0	100

Table 5.5 Blend combination of NR and CNR with CSM rubber

CSM (phr)	NR/CNR (phr)[a]
100	0
80	20
60	40
40	60
20	80
0	100

Cure system: zinc oxide 5; stearic acid 2; sulfur 1.5; tetramethylthiuram disulfide (TMTD) 2; magnesium oxide 4

[a]Part per hundred parts of rubber

Table 5.6 Formulation of the cross-linked systems based on acrylonitrile butadiene rubber (NBR), polychloroprene rubber (CR), chlorosulfonated polyethylene rubber (CSM), and nano- and micro-particle-sized SiO_2-filled NBR/CSM and CR/CSM cross-linked systems

Compounds/phr[a]	1	2	3	4	5	6	7	8	9
NBR[b]	100	–	50	50	50	–	–	–	–
CSM[c]	–	100	50	50	50	–	50	50	50
CR[d]	–	–	–	–	–	100	50	50	50
ZnO	5	5	2.5	2.5	2.5	5	2.5	2.5	2.5
Stearic acid	2	2	2	2	2	2	2	2	2
SiO_2^e	–	–	–	35	–	–	–	35	–
SiO_2^f	–	–	–	–	35	–	–	–	35
Naphthenic oil[g]	–	–	–	11	11	10	10	10	10
MgO[h]	–	4	2	2	2	–	2	2	2
ETU[i]	–	–	–	–	–	1	0.5	0.5	0.5
TMTD [j]	2.5	2	2.5	2.5	2.5	–	1	1	1
CZ [k]	2		1	1	1	–	–	–	–
S	0.5	1	0.75	0.75	0.75	–	0.5	0.5	0.5
Diethylene glycol	–	–	–	1.1	1.1	–	–	1.1	1.1

[a]Part per hundred parts of rubber, [b]Butadiene–acrylonitrile copolymer rubber–Europren N3345, [c]Chlorosulfonated polyethylene rubber—Hypalon 40S, [d]Polychloroprene rubber—Baypren 110, [e]White filler (15 nm)—Ultrasil VN 3, [f]White filler (28 μm)—Celite 281, [g]Naphthenic oil—TEPHIL NAPHTHENE P. O. 100, [h]Magnesium oxide—Anscor P, [i]Ethylene thiourea—ETU, [j]Very fast accelerator—tetramethylthiuram disulfide (TMTD), [k]Low fast accelerator—N-cikloheksil-2-benzothiazole sulfenamide(VULKACIT CZ)

an angular displacement of ± 3 and a frequency of 1.7 Hz [20]. The cure rate index (CRI) is the measure of rate of vulcanization based on the difference between optimum cure time of vulcanization t_{c90} and the scorch time t_{s2}. It can be calculated from the relation:

$$\text{CRI} = \frac{1}{t_{c90} - t_{s2}} \times 100 \qquad (5.2)$$

5.3.2 Mechanical Properties

The sheets were cut, marked according to the time and temperature determined from the oscillating disk rheometer, and vulcanized in clean polished molds in a press at 160 °C. The vulcanized sheets were cut into dumbbell-shaped specimens (five replicates from each sample) for the evaluation of the mechanical properties using an electronic tensile testing machine (Zwick 1425, Germany) at a speed of 500 mm/min. Samples of at least 0.12 mm in thickness with flat surface were cut for hardness test. The measurement was carried out according to ASTM D 2240 using durometer of model 306L type. The tensile properties were determined using the tensile testing machine type Zwick 1445 according to ASTM D-412. The average value of the mechanical properties was calculated using at least three samples. A cross-head speed of 50 mm/min was used, and the tests were performed at 25 °C.

5.3.3 Hardness Measurements

Samples of at least 0.12 mm in thickness with flat surface were cut for hardness test. The measurement was carried out according to ASTM D 2240 using durometer of model 306L type. The unit of hardness is expressed in (Shore A).

5.3.4 Swelling Measurements and Cross-linking Density Determination

The investigated rubber composites were obtained as small sheets (1 g) weighed accurately and immersed in a 25 cm^3 benzene solvent in closed simple bottles, at 25 °C. After 72 h, the samples were removed from the solvent and weighed in a glass-stopper bottle after removing the surface fluids by blotting with a filter paper. The volume swelling in percentage was calculated using the following equation [21]:

$$R_v = 1 + [(w - w_0) - 1]\rho_r/\rho_s \qquad (5.3)$$

$$R_w = w/w_0 \qquad (5.4)$$

$$v_2 = 1/R_v \qquad (5.5)$$

where R_v and R_w are the volume and mass ratio of rubber samples in the swollen gel; w and w_0 are weights of the sample before and after swelling, respectively; ρ_r and ρ_s are densities of the rubber and the solvent, respectively; and v_2 is the volume fraction of the sample in the swollen gel. The elastic modulus (E) values were

obtained from dumbbell samples by stress–strain measurements [22] . The values of E were obtained from the initial slope of the curves in neo-Hooke's stress–strain relation σ versus (α and α^{-2}) in the equation below:

$$\sigma = E\left(\alpha - \alpha^{-2}\right) \tag{5.6}$$

where α is the elongation ratio (L/L_0).

The E modulus is related to cross-linking density by the well-known equation from the kinetic theory of elasticity:

$$E = gvRT \tag{5.7}$$

where the factor $g < 1$, n is the concentration of cross-linking density, R is the universal gas constant, and T is the absolute temperature.

$$v = \rho/M_c \tag{5.8}$$

$$M_c = \rho RT/E \tag{5.9}$$

where M_c is the average molecular weight between two cross-links. The Flory–Huggins interaction parameter, w, was calculated for the rubber composites in a benzene solvent, according to the formula below:

$$x = \left[vV_1\left(v_2^{1/3} - 0.5v_2\right) + \ln(1 - v_2) + v_2\right]/v_2^2 \tag{5.10}$$

where V_s is the molar volume of the benzene solvent. Cross-linking density was determined from the swelling data. The samples were allowed to swell in the benzene solvent, and the equilibrium uptake was noted. The molecular weight between the cross-link M_c was calculated using the following equation:

$$M_c = -2V_1\rho_r V_r^{1/3}/\ln(1 - V_r) + V_r + 2x^2V_1^2 \tag{5.11}$$

where M_c is the molecular weight of the polymer between two cross-links; ρ_r is the rubber composite density; V_s is the molar volume of benzene solvent; V_r is the volume fraction of rubber composites; and w is the filler–polymer interaction parameter. The Kraus model, used for the investigation of the filler–rubber interaction, shows how to quantitatively calculate the effect of particles that are either completely unbound or completely and permanently bound to the polymer. The Kraus equation is given in the equation [23]:

$$\frac{V_{r0}}{V_{rf}} = 1 - [m\theta/(1 - \theta)] \tag{5.12}$$

$$m = 3C\left(1 - V_{r0}^{1/3}\right) + V_{r0} - 1 \tag{5.13}$$

where V_{r0} and V_{rf} are the volume fraction rubber in the solvent-unfilled and solvent-filled rubber composites; y is the volume fraction of the filler in the rubber composites; the parameter m is obtained from the graphic V_{r0}/V_{rf} versus $\Theta/1 - \Theta$ and describes how the swelling of polymer matrix decreases when the filler content increases; and C is the constant characteristic for the filler, but it depends on the solvent.

5.3.5   Morphological Study Using a Scanning Electron Microscope

SEM images were obtained using a JEOL 5300 SEM operated at an acceleration voltage of 20 kV and equipped with energy-dispersive systems. All the studied samples were coated with a thin layer of gold in a nitrogen atmosphere.

5.3.6   Thermal Stability

Thermogravimetric (TG) measurements have been performed on the PerkinElmer TGS-2 instrument. Rubber samples were heated from 25 to 750 °C at a heating rate of 10 °C min^{-1} in the nitrogen atmosphere with the gas flow rate of 50 cm^3 min^{-1}. The mass of the samples ranged from 17 to 25 mg.

5.3.7   DSC Measurements of Rubber Blends

The thermal stability of pure CR/CSM rubber blend and CR/CSM rubber blends filled with nano- and micro-silica particles was investigated by non-isothermal thermogravimetric analysis (TG) using a PerkinElmer TGS-2 instrument. The measurements were conducted at heating rates of 10 °C min^{-1} in a dynamic nitrogen atmosphere (flow rate 25 cm^3 min^{-1}), in the temperature range from 25 to 750 °C. The average sample mass was about 8 mg.

5.3.8 Dynamic Mechanical Analysis (DMA)

Dynamic mechanical properties were studied on a mechanical analyzer Tritec 2000 (Triton Technology). Complex Young's modulus $E^* = E' + iE''$ (E' is a storage and E'' loss modulus) was measured in a single cantilever bending mode. Temperature dependencies of dynamic mechanical properties were measured at a heating rate of 2 °C/min in the temperature range from −50 to 150 °C at 5 frequencies (0.31; 1; 3.1; 10; and 31 Hz). Multifrequency mode was used to determine a dependence of E^* on frequency (f) at frequency f = 1 Hz. Cross-linking density can be obtained using DMA by calculating M_c, the (number) average molar mass of elastically effective chains (between cross-links), according to the following equation derived from the theory of rubber elasticity [24, 25]:

$$E = 3\rho RT/M_c$$

where E is the elastic modulus in the rubbery plateau (assimilated to the storage modulus E^* measured at 1 Hz), R the gas constant, T the absolute temperature, and q the material density at T.

5.3.9 FTIR Analysis

Fourier transform infrared spectra (FTIR) were recorded on a Bruker IFS-66 spectrometer with an attenuated total reflection (ATR) attachment. The internal reflection element (IRE) chosen was a 45° KRS-5. Samples for measurements were approximately 0.3-mm-thick sheets, prepared by compression molding between two Teflon films at a temperature of 100 °C.

5.4 New Challenges

5.4.1 Nano- and Micro-silica-Filled CR/CSM
Rubber Blends

The nano-silica-filled CR/CSM rubber blends have higher values for cure characteristics than micro-silica particle-sized filled compounds. Nano-silica type activated the vulcanizing process through the promotion of hydrogen sulfide formation and the rupture of S–N linkage when heated with sulfonamides in rubber either in the presence or in the absence of other compounding ingredients. The strong peak from SiO–C at 1070 and 1079 cm^{-1} in the IR spectrum of nano- and micro-silica-filled CR/CSM rubber blend suggested the presence of interaction with silica which

leads to increased stability of the filled CR/CSM polymer blends. According to the Kraus equation, it can be observed that the nano-silica-filled CR/CSM rubber blend has higher Vr_0/V_{rf} values and better rubber filler interactions than that micro-silica-filled composites. The higher values of the glass transition temperatures for the nano- than the micro-filled cross-linked systems are indicated by DMA analysis. The density of the nano-silica-filled CR/CSM rubber blends was lower than that of the micro-silica-filled and was transparent at all filler concentration.

5.4.2   Cure Characteristics

The maximum and minimum torque (M_h and M_l) and delta torque (ΔM) at 160 °C (Table 5.7) increase with the increase of the nano- and micro-silica loading filler of the CR/CSM cross-linking systems. The difference between M_h and M_l could be used as an indirect indication of the cross-linking density of the rubber compound [26]. Both scorch time (t_{s2}) and optimum curing time (t_{c90}) are found to decrease noticeably with increasing silica loading. The nano-silica particle-sized filled rubber blends have higher values than micro-silica particle size for all cure characteristics.

5.4.3   IR Spectral Analysis

ATR spectra carried out on samples of pure CR/CSM rubber blend and of two composites with two different silica particle size contents are displayed in Fig. 5.1 (spectrum 1, 2, and 3). The assignment of the principal bands is presented in Table 5.8. Almost all bands [27] of the pure polymer blend especially those associated with the stretching bands of the CH_2 groups are shifted to lower wave numbers in the filled polymer blend spectra. The bands located at 2943 and 2862 cm^{-1}, respectively, assigned to the asymmetric and symmetric stretch of the methylene group, are found at 2943 and 2860 cm^{-1} for the nano-silica-filled CR/CSM composite and at 2926 and 2858 cm^{-1} for the micro-silica-filled CR/CSM

Table 5.7 The cure characteristics of unfilled and nano- and micro-silica particle-sized filled CR/CSM compounds

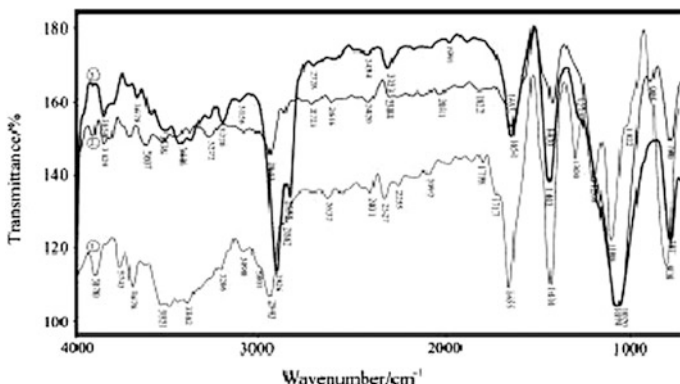| Cure characteristics	Sample						
	1	2	3	4	5	6	7
M_h (dNm)	38	34	41	47	37	34	39
M_l (dNm)	8	10	11	13	8	8	8
ΔM (dNm)	30	24	30	34	29	26	31
t_{s2} (min)	2.32	3.25	3.13	2.38	2.14	1.59	1.39
t_{c90} (min)	23.08	19.15	20.21	21.15	21.5	23.07	16.24

Fig. 5.1 FTIR ATR spectrum of (*1*) unfilled, (*2*) nano-, and (*3*) micro-silica particle-sized filled polychloroprene (CR) and chlorosulfonated polyethylene (CSM) rubber blends CR/CSM (50/50 w/w)

composite sample. The absorption band at 1108 cm^{-1} in the cross-linked CR/CSM rubber blend is assigned to symmetric vibration of SO_2 group.

The peak of –S–Cl which is attributed to the –SO_2Cl group from CSM is absent, and the peak of –C–Cl from CR rubber is absent also. This suggests the cross-linking of the rubber blend macromolecules. Similar observations were made by Ahankaria et al. [28] with reference to the thermally induced self-cross-linking PVC/CR, as well as the PVC/CSM.

The absorption bands at 1655 and 1434 cm^{-1} in the cross-linked CR/CSM rubber blend are assigned, respectively, to symmetric and asymmetric bending vibration of C=C group. The weak absorption bands at 3536 and 3446 cm^{-1} which are attributed to hydrogen bands are strongly attenuated by reaction macro-molecules and fillers. New absorption bands centered at 1070 and 1079 cm^{-1} could be assigned to the symmetric stretching modes of SiO–C group from silica filler, and moving symmetric and asymmetric bending vibration of C=C group from 1655–1651 to 1653 cm^{-1} and from 1434–1430 to 1445 cm^{-1} (Fig. 5.1, spectrum 2 and 3) suggests the interaction of the polymers matrix with the silica, also.

5.4.4 Mechanical Properties

Table 5.9 represents the effect of nano- and micro-silica loading on tensile properties (tensile strength, modulus, and elongation at break) and hardness of the rubber vulcanizates. The tensile strength increases with increasing nano- and micro-silica loading in CR/CSM rubber compound. Maximum value of tensile strength, for nano-silica-filled CR/CSM rubber compound, is by samples 4 and 7 with 35 phr nano- and micro-silica (15.8 and 8.5 MPa). The improvement in tensile properties for nano-silica-filled composites seems to be responsible for the

Table 5.8 FTIR-ATR spectroscopic data for unfilled and nano- and micro-silica particle-sized filled polychloroprene (CR) and chlorosulfonated polyethylene (CSM) rubber blends CR/CSM (50/50 w/w)

	Wave number (cm^{-1})	Group	Assignment
CR/CSM (50/50 w/w) rubber blends	2943	CH$_3$–, –CH$_2$–, > CH–	v(–C–H)
	2862	CH$_3$–, –CH$_2$–, > CH–	v(–C–H)
	1655	–CH=CH–	v(–C=C)
	1434	RHC=CHR	δ(–C–H)
	1108	–SO$_2$–	v(SO$_2$)$_{sym}$
CR/CSM/nano-silica rubber blend	2943	CH$_3$–, –CH$_2$–, > CH–	v(–C–H)
	2860	CH$_3$–, –CH$_2$–, > CH–	v(–C–H)
	1655	–CH=CH–	v(–C=C)
	1430	RHC=CHR	δ(–C–H)
	1108	–SO$_2$–	v(SO$_2$)$_{sym}$
	1070	SiO–C	v(SiO–C)
CR/CSM/micro-silica rubber blend	2926	CH$_3$–, –CH$_2$–, > CH–	v(–C–H)
	2858	CH$_3$–, –CH$_2$–, > CH–	v(–C–H)
	1651	–CH=CH–	v(–C=C)
	1445	RHC=CHR	δ(–C–H)
	1108	–SO$_2$–	v(SO$_2$)$_{sym}$
	1079	SiO–C	v(SiO–C)

v—stretching vibrations; δ—bending vibrations in plane

Table 5.9 Some mechanical properties of unfilled and nano- and micro-silica particle-sized filled CR/CSM compounds

Characteristics	Sample						
	1	2	3	4	5	6	7
Tensile strength (MPa)	6.4	13.6	14.6	15.8	6.6	8.3	8.5
Elongation at break (%)	688	572	523	485	600	600	549
Hardness, Shore A	57	65	69	71	55	55	55
Modulus at 300 % elongation (MPa)	2.8	6.5	7	7.1	2.8	3	3

improved dispersion of the nano-silica into the rubber matrix, leading to a higher bound rubber formation [29]. The values of 300 % modulus are increased from 6.5 to 7.1 MPa for nano-silica and 2.8 to 3 MPa for micro-silica-filled compounds, strongly attenuated by reaction macromolecules and fillers, respectively. The hardness values of micro-silica-filled compounds are the same and much lower than nano-silica-filled compounds as shown in Table 5.9.

Values of elongation at break are decreasing with increasing silica loading. The increase of hardness, modulus, and tensile strength and higher values for nano- than micro-silica composites can possibly be explained by the improvement of the degree of adhesion at interfaces between the nano-silica and the CR/CSM rubber blends.
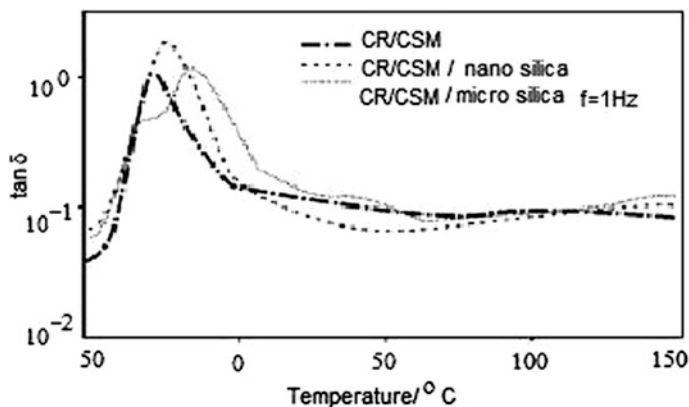
Fig. 5.2 Damping properties (tanδ) as a function of temperature of the unfilled and nano- and micro-silica particle-sized filled CR/CSM (50/50) rubber blend

Table 5.10 The glass transition temperatures (T_g) estimated either by dynamical spectroscopy (T_{gm}), the modul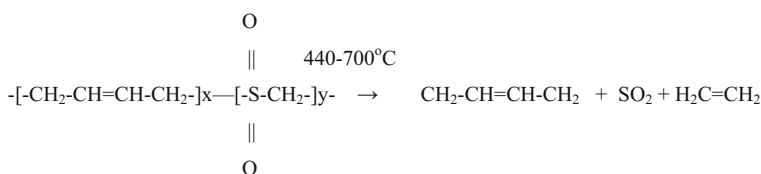us of elasticity (G), determined from stress strain measurements and cross-linking density (v), calculated from the storage modulus E' (at 70 °C, 1 Hz) or (V) determined by swelling

Compounds	Sample		
	1	4	7
T_{gm} (1 Hz)/°C	−21	−29	−16
G (MPa)	6.4	15.8	8.5
$E'/10^3$ MPa	5.2	18.1	7.5
V/mol m^{-3}	553	646	173
N_c/mol m^{-3} (from E')	1115	933	756

5.4.5 Dynamic Mechanical Analysis

Dynamic mechanical analysis (DMA) is based on the differences in mechanical damping properties of unfilled and filled rubber vulcanizates [30]. Figure 5.2 and Table 5.10 show the elastic modulus, E_0, and tan$d$ determined from a dynamic mechanical analyzer under the conditions of 1 Hz and 0.1 % dynamic strain amplitude. The addition of filler to rubber matrix would lower the peak value of tan$d$, designated as (tanδ_{max}), in the plot of tanδ versus temperature. E_0 of blends increases significantly with the addition of silica, particularly at a temperature above the CR/CSM rubber blend glass transition temperature (T_g). This result indicates a strong reinforcement caused by strong interaction between silica and CR/CSM rubber blend via silanol groups and chlorine atoms, respectively (Table 5.10) [31]. Values of glass transition temperature (T_g) determined from the damping peak tanδ are summarized in Table 5.10. In theory, the shift in T_g would be caused by silica–polymer interaction and/or a change in phase compatibility.

Table 5.11 The cross-linking density of unfilled and nano- and micro-silica particle-sized filled CR/CSM compounds

Parameters	sample						
	1	2	3	4	5	6	7
r_p (g cm^{-3})	1.23	1.27	1.3	1.3	1.13	1.16	1.17
R_w	1.07	1.69	1.74	1.07	2.03	1.84	1.07
R_v	1.09	1.22	1.2	1.06	1.21	1.1	1.06
V (mol m^{-3})	553	231	430	646	391	242	173
M_c (gmol^{-1})	1115	2749	1580	1008	1621	2683	3884

5.4.6 Cross-linking Density

The values of R_W and R_V (Table 5.11) decrease with increasing amount of both nano- and micro-silica.

The cross-linking density, V, increased with increasing silica concentration and was the largest for the sample containing nano- and micro-silica of 35 and 10 phr, respectively (samples 4 and 5). The largest chain molecular mass was obtained for micro-silica-filled compounds with amount of 35 phr (sample 7) and the smallest for the sample 4 with the highest amount of nano-silica. The swelling degree decrease can be explained by linkage combination between polymer chains and functional groups on the silica surface and by a possible increase in cross-linking bonds in the polymer matrix because of filler influence on the vulcanization reaction [32]. The cross-linking density (v) of the nano- and micro-silica particle-sized filled CR/CSM rubber blend was calculated from the equilibrium storage modulus in the rubber region over the α-relaxation temperature according to the rubber elasticity theory. The correlations of some data for the modulus of elasticity (G) determined

Fig. 5.3 Plot of V_{ro}/V_{rf} versus $\phi(1 - \phi)$ according to the Kraus equation for swelling test of nano- and micro-silica particle-sized filled CR/CSM (50/50) rubber blend
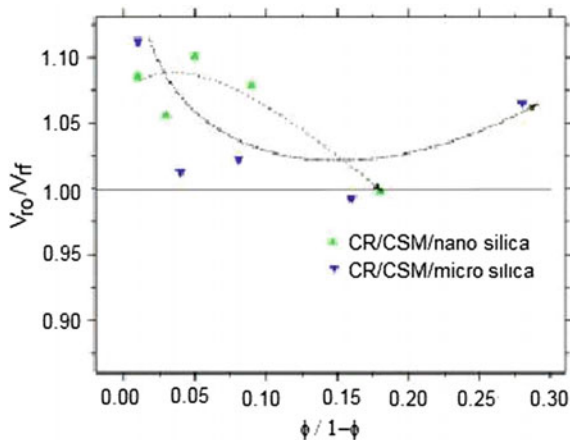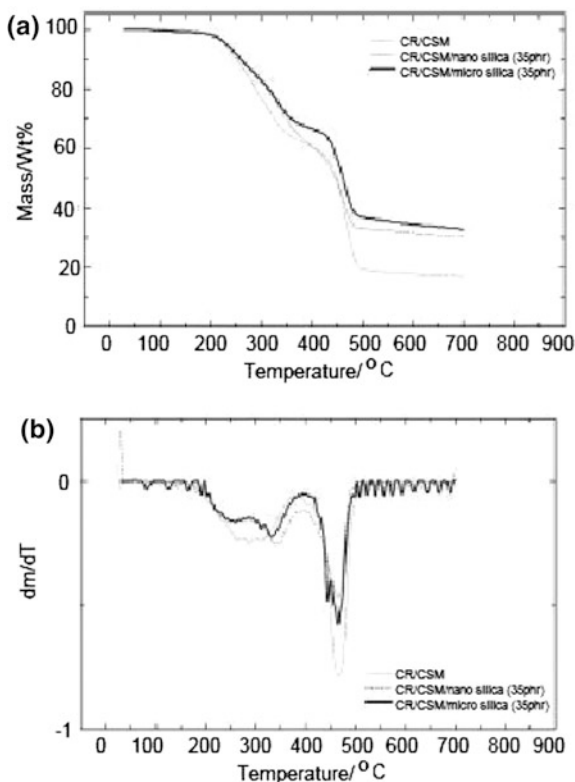
from stress–strain measurement and cross-linking density (v) calculated from the storage modulus E_0 (at 70 °C, 1 Hz) or (V) determined by swelling are included in Table 5.10. Figure 5.3 shows the plot of V_{r0}/V_{rf} versus $\phi/(1 - \phi)$ according to the Kraus equation [33]. It can be observed exhibit deviations from the proposed linear model, which are greater than 1.

As filler loading increases, the ratio of V_{r0}/V_{rf} decreased. The nano-silica-filled CR/CSM rubber blend has higher V_{r0}/V_{rf} values than micro-silica composites and show better polymer–filler interaction. Thermal stability of CR/CSM compounds filled with nano- and micro-silica particle size. The thermal stability of pure CR/CSM rubber blend and CR/CSM rubber blends filled with nano- and micro-silica particles has been discussed. The thermal decomposition of CR/CSM rubber blend and nano- and micro-silica particle-sized filled CR/CSM rubber blends occurs generally in two main stages (Fig. 5.4a, b; Table 5.12). The first step degradation occurs in the temperature region 250–300 °C, and the second-step degradation is about at 440 °C. The data for the initial decomposition temperature (IDT) (5 % mass loss) [34] and 10 and 30 % mass loss temperatures are given in Table 5.12 and Fig. 5.4a. It can be seen that according to the IDT nano-silica-filled CR/CSM compounds are more stable than unfilled and micro-silica-filled

Table 5.12 Temperature values of unfilled and nano- and micro-silica particle-sized filled CR/CSM compounds for selected mass loss (5, 10, and 30 %)

Compounds	Sample						
	1	2	3	4	5	6	7
DTG peak values (°C)	293.79	326.51	330.35	343.01	334.16	328.87	332.17
	464.64	467.77	468.15	465.14	46.2	459.81	464.51
Mass loss (%)	21.15	26.96	25.44	27.93	24.76	25.67	24.36
	61.58	47.67	58.28	56.85	62.06	50.63	52.66
Total mass loss (%)	84.01	75.73	71.57	69.91	77.52	73.59	67.17
Temperature values for selected mass loss							
$T_{5\%}$ (°C)	225.67	227.81	232.53	233.25	230.5	231.01	232.02
$T_{10\%}$ (°C)	251.61	241.77	262.16	236.3	247.39	254.42	238.64
$T_{30\%}$ (°C)	326.14	353.17	351.45	347.93	338.99	345.12	358.48

$$-[-CH_2-CH=CH-CH_2-]x—[-S-CH_2-]y- \xrightarrow{440-700°C} CH_2-CH=CH-CH_2 + SO_2 + H_2C=CH_2$$

(with S bearing two O via double bonds: $\overset{O}{\underset{O}{\overset{\|}{\underset{\|}{S}}}}$)

Scheme 5.1 Decomposition mechanism of CR/CSM rubber blend

compounds. In the next step (at 10 % mass loss) with 20 phr of nano-silica and 30 phr of micro-silica particle-sized filled CR/CSM rubber have higher temperature values (262 and 259 °C) than other samples. At 30 % mass loss, the CR/CSM rubber blends filled with 20 phr of nano-silica and 30 phr of micro-silica particle size are the most stable also than other compounds. Figure 5.4a, b shows that unfilled CR/CSM rubber blend compounds are initially more stable than other samples. In the CR/CSM rubber blend compounds filled by nano- and micro-silica types (Table 5.12; Scheme 5.1), the degradation takes place in two stages. Up to 100 °C, there is no change and hence no mass loss. The first-step degradation occurs in the temperature region 250–350 °C and the mass loss in the range 21.15–27.93 and 21.15–28.76 % (depending on the type and amount of silica in CR/CSM rubber blends), most probably indicating the evaporation of oil (naphtalene). The second-step degradation starts at 440 °C and ends at 700 °C. The percent of mass loss at this region is in the range of 47.67–61.58 and 52.66–62.06 % for nano- and micro-silica-filled CR/CSM rubber blend indicating polymer degradation. The large flexible polysulfidic linkages undergo chain scission and convert into monosulfidic and disulfidic linkages. Synthetic rubber decomposes by random chain scission with intramolecular hydrogen transfer. Table 5.12 presents the DTG peak values of CR/CSM rubber compounds filled by nano- and micro-silica particle size. DTG

peaks shift to higher temperature values indicating greater thermal stability of samples containing 20 phr nano and micro silica.

Morphology Microscopic Studies

Scanning electron microscopic (SEM) studies of fractured surfaces were observed by scanning electron microscopy (SEM) in order to gain a better insight into the mechanism of failure of SiO_2-reinforced NBR/CSM and CR/CSM cross-linked systems. The SEM microphotographs at 2000 magnification of the surfaces of

Fig. 5.5 SEM micrograph at 2000× magnification of CR/CSM rubber blends: **a** micro-silica and **b** nano-silica filled
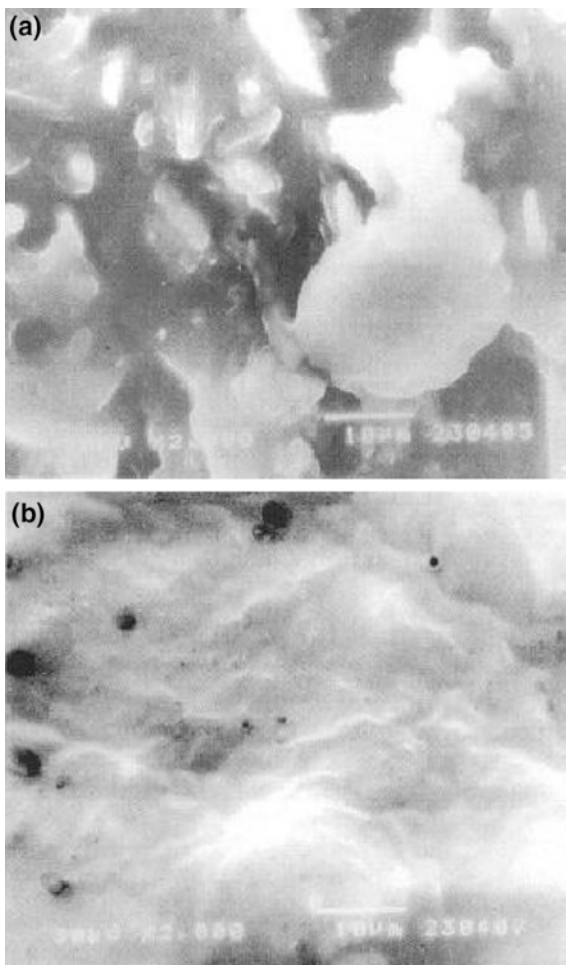
CR/CSM polymer blends are shown in Fig. 5.5. The surface of the CR/CSM polymer blend with nano-SiO$_2$ is more polished than that with micro-SiO$_2$. In the microphotographs of micro-SiO2-filled CR/CSM blend a micro-crack of size about 50 μm can be seen.

5.4.7 SBR/CSM/ Carbon Black Rubber Composites

For SBR/CSM blends, the addition of filler leads to a significant enhancement in the physical properties if CSM is the major blend constituent. The blends containing CB N339 show higher hardness, tensile strength, and abrasion resistance when compared to the ones containing CB N772. The experimental data indicate that this can be caused by the improvement in the polymer–filler phase bonding which results from the interfacial interaction of functional groups of the polymer and the active sites of the filler surface leading to a higher apparent cross-linking density. As the concentration of CSM in the rubber blend increases, the cure characteristics, such as optimum cure time, scorch time, and induction time at 160 °C, increase for the blends filled with CB N339. The results for the curing behavior are consistent with the mechanical properties of the SBR/CSM blends.

5.4.8 Mechanical Properties

It was shown that for SBR/CSM blends, the addition of filler leads to a significant enhancement in the physical properties if CSM is the major blend constituent. The blends containing CB N339 show higher hardness, tensile strength, and abrasion resistance when compared to the ones containing CB N772. The experimental data indicate that this can be caused by the improvement in the polymer–filler phase bonding which results from the interfacial interaction of functional groups of the polymer and the active sites of the filler surface leading to a higher apparent cross-linking density. As the concentration of CSM in the rubber blend increases the cure characteristics, such as optimum cure time, scorch time and induction time at 160 °C increases for the blends filled with CB N339. The results for the curing behavior are consistent with the mechanical properties of the SBR/CSM blends. Figure 5.6 shows a comparison of the evolution of the hardness of SBR/CSM blends reinforced by the two types of highly structured carbon black (N339 and N772). It can be seen that the hardness of the blend increases in both systems when the content of CSM rubber increases. However, the increase of the hardness is much more pronounced in the case of the active filler N339 than in the one where N772 was used. Above 50 % of CSM in the blend, the hardness tends to reach a plateau value for N339, whereas it passes through a maximum in the blends filled with N772. The volume fraction of CB affects the mechanical properties of the polymer blends positively [35].

Fig. 5.6 The influence of
CSM rubber content on
hardness of rubber blends
reinforced by highly
structured carbon black, with
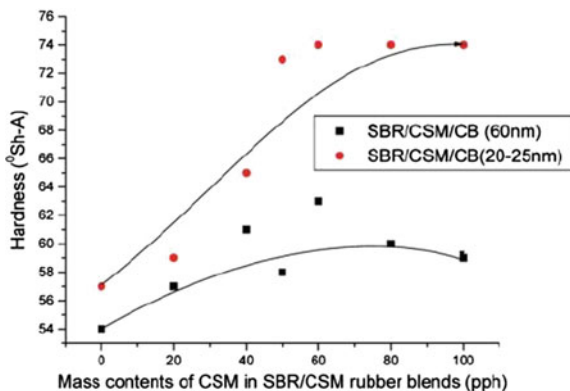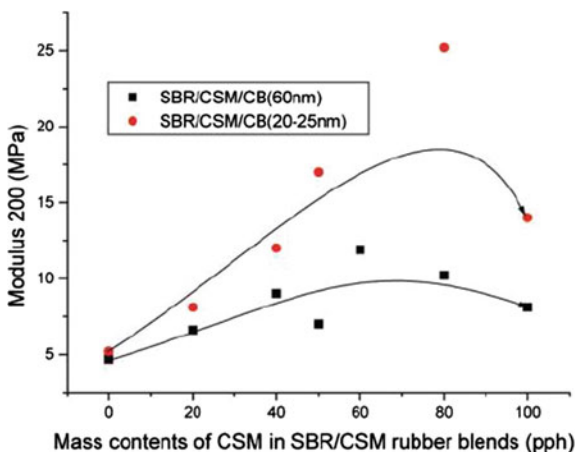the primary particle size either
20–25 nm or 60 nm

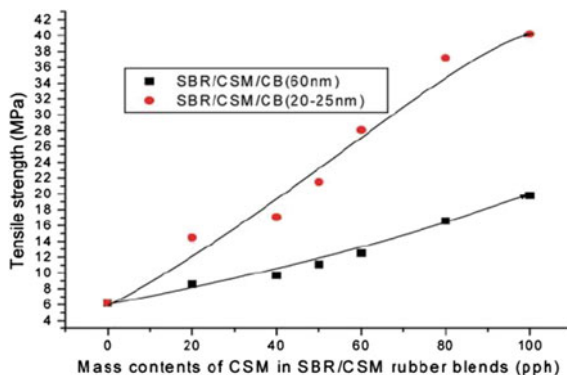**Fig. 5.7** The influence of
CSM rubber content on
modulus 200 of rubber blends
reinforced by highly
structured carbon black, with
the primary particle size either
20–25 nm or 60 nm

The relationship between the tensile strength, the modulus (M200) at 200 %
elongation and the elongation at break (Eb) and the content of CSM in the blends is
shown in Figs. 5.7, 5.8, 5.9, and 5.10. All the figures show increasing physical
properties with the increasing CSM content in the blend. Again, the reinforcement
by CB with smaller primary particle size becomes evident. If the modulus 200 is
considered, it becomes evident that the targeted value for SBR/CSM/CB 339 passes
a maximum value, whereas for SBR/CSM/N339, the modulus tends to a limiting
value (Fig. 5.7).

The reinforcement by CB is shown evidently by the evolution of the tensile
strength (Fig. 5.8). For SBR/CSM/CB N339, the values range from 6 to 39 MPa. In
comparison with that, the effect of the more coarse black N772 increases the tensile
strength from 6 to 18 MPa only. In both cases, the tensile strength increases
approximately linearly with the content of CSM in the blend, indicating a prefer-
ential distribution of the CB into this polymer phase. If the elongation at break is

Fig. 5.8 The influence of CSM rubber content on tensile strength of rubber blends reinforced by highly structured carbon black, with the primary particle size either 20–25 nm or 60 nm


Fig. 5.9 The influence of CSM rubber content on elongation at break of rubber blends reinforced by highly structured carbon black, with the primary particle size either 20–25 nm or 60 nm
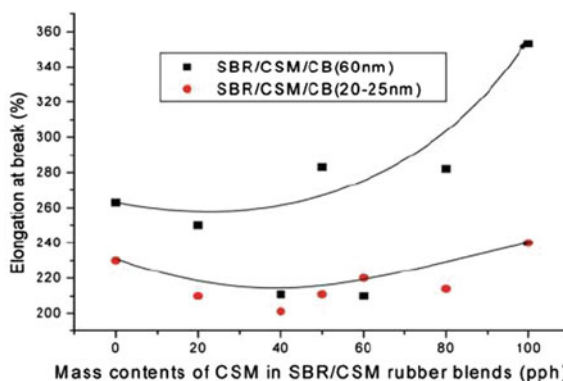
considered (Fig. 5.9), it is shown from Fig. 5.8 that the values remain unchanged until 40–50 % of CSM in the blend is reached. After this threshold, the values increase strongly when the CSM content increases. In addition, a slight inversion of the reinforcing effects can be observed. The lower values (about 200 and 240 %) were obtained for systems reinforced by CB N339, and significantly higher values (260 and 350 %) were recorded for all systems reinforced by CB N772. As an overall picture, it seems that the values of tensile properties and elongation at break are synergistic above 50 % CSM leading to higher energies at break. The values gained for the abrasion loss are illustrated in Fig. 5.10. Despite the higher scatter of the experimental data, it can be shown that (i) the abrasion loss is higher for the compounds containing CB N772 than for the ones containing CB N339. However, as a systematic picture in both groups of compounds, the abrasion loss is passing through a maximum at 40–50% CSM underlining again the effect of the reinforcement in the range of high CSM concentrations. More details about the values of the specific mass are tabulated in Table 5.13. It can be seen from this table that the specific mass ranges from 1.082 to 1.312 g/cm^3. The reason for this could be differences in the dispersion and distribution of the fillers in rubber blend.

Fig. 5.10 The influence of
CSM rubber content on
abrasion loss of rubber blends
reinforced by highly
structured carbon black, with
the primary particle size either
20–25 nm or 60 nm
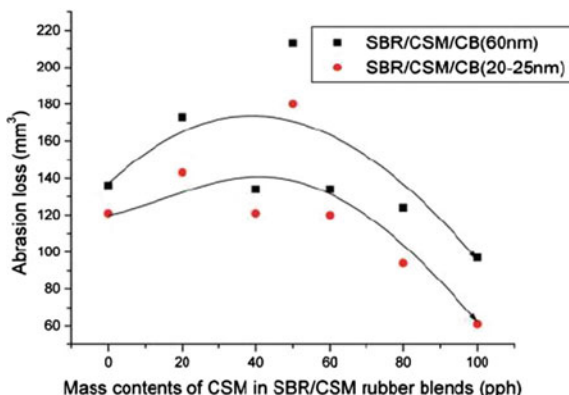
Table 5.13 Curing characteristics and experimental values of specific mass of rubber blends reinforced highly structured carbon black with the primary particle size was either 20–25 nm or 60 nm at 160 °C

Sample name	Maximum torque (M_h) (dNm)	Minimum torque (M_l) (dNm)	Scorch time at 160 °C, t_{s2} (min)	Optimum cure time at 160 °C, t_{c90}, (min)	Cure rate index (CRI) (min^{-1})	Specific mass (g/cm^3)
1	15	5	2.5	15	0.08	1.08
2	19	4.5	5.3	11	0.17	1.11
3	25	8.5	8	23	0.06	1.14
4	28	5	9.8	21	0.09	1.15
5	29	5	10	30	0.05	1.17
6	29	4	10.5	21	0.09	1.21
7	32	4	4.7	19	0.07	1.25
8	33	4	6.8	12	0.18	1.12
9	38	4	5	16	0.09	1.25
10	38	5	4	14	0.1	1.27
11	38	5	4	19	0.07	1.29
12	39	5	4	17	0.07	1.3
13	39	4	5	16	0.09	1.31
14	32	4	4	19	0.07	1.31

Equilibrium swelling measurements were performed in order to evaluate the apparent cross-linking density in the blend compound, which contains the contribution of the chemical cross-links as well as the one of the strong physical attachments of the polymer to the filler. The values of the cross-links density calculated by using Eq. 5.14 are given in Fig. 5.11. A clear linear increase of the apparent cross-linking density with the CSM content in the blend was observed irrespective of the type of carbon black used. This indicates as the major contributor a strong interaction between the functional groups of CSM and the filler leading to

Fig. 5.11 Relation between cross-linking density ν values and CSM mass content of SBR/CSM rubber blends reinforced by highly structured carbon black with the primary particle size either 20–25 nm or 60 nm
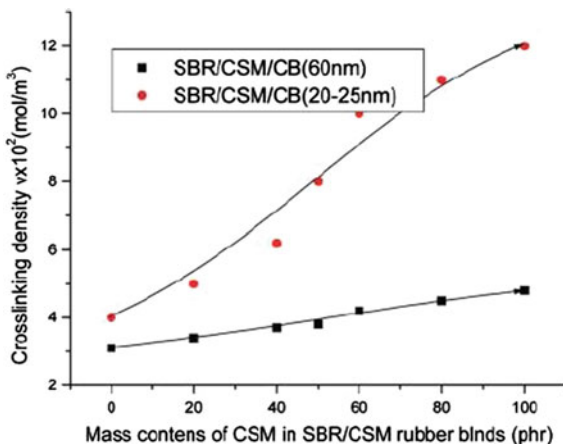
strong physical cross-links and eventually also chemical ones which are not affected by the polar solvent used.

$$\nu_{EANC} = \rho_p N_A / M_c \qquad (5.14)$$

$$M_c = -V_1 \rho_p \frac{\left(\varphi_p^{1/3} - \frac{\varphi_r}{2}\right)}{\ln\left(1 - \varphi_p\right) + \varphi_p + x_p + x_1 \varphi_p^2} \qquad (5.15)$$

These results are to some extent supported by the observations of the curing characteristics. The maximum torque, the optimum cure time, and the scorch time change significantly with the blend composition. However, concerning the influence of the filler there were no much differences in the scorch and cure time of the blends filled with CB N339 and CB N772. The minimum torque values are for all the compounds in the same range, irrespective of the CSM content in the rubber blends. There was also no difference in the M_l values of the materials filled with CB N339 and the ones filled with CB N772. However, concerning the M_h values, there are two groups of values which show a certain influence by the type of the filler used. For the CB N339, the M_h values increase significantly when the CSM content increases. This behavior is not observed for the group of compounds filled with CB N772. Differences occur between the M_h values of the two series of compounds.

This difference can be caused by a more effective interfacial adhesion between CSM and the active CB. At the micro-level, physical and chemical interactions between the functional groups of CSM and the active sites of the high surface specific area CB can lead to a higher apparent cross-linking density. The formation of a greater number of interfacial cross-links may occur. As the concentration of

CSM in the blend increases, the cure characteristics such as optimum cure time, scorch time, and induction time at 160 °C increase for the blends filled with CB N339. Therefore, the optimum cure time increases. Thus, the results are consistent with the ones from the mechanical behavior.

5.4.9 NR/CSM and NBR/CSM Rubber Blends Reinforced by Carbon Black

The influence of carbon black (with an average particle size of 40 nm) on NR/CSM and NBR/CSM rubber blends reinforced by carbon black was investigated. The mechanical properties of elastomer depend mainly on the carbon black loading. Tensile strength, modulus at 100 % elongation, and hardness were increased with increasing radiation dose, as well as carbon black loading, but the elongation at break values decreases with increasing radiation dose and carbon black content. The FTIR spectra of aged samples confirmed the formation of various oxidation products, i.e., alcohols, ethers and small amounts of lactones, anhydrides, esters, and carboxylic acids during radiation. Significant changes in spectra are induced by chain scission which was registered in the 1620–1450 cm^{-1} region. The formation of shorter polyene sequences and aromatic rings is assumed. The radiation doses lower than 100 kGy influenced only small changes in the rubber macromolecules structure if we consider the development of the bands in carbonyl and conjugated C=C bond regions. On the other hand, 200, 300, and 400 kGy doses caused a serious chemical modification of the prepared rubber blend samples.

Fig. 5.12 Rheometric curves for curing of unfilled and filled rubber blends
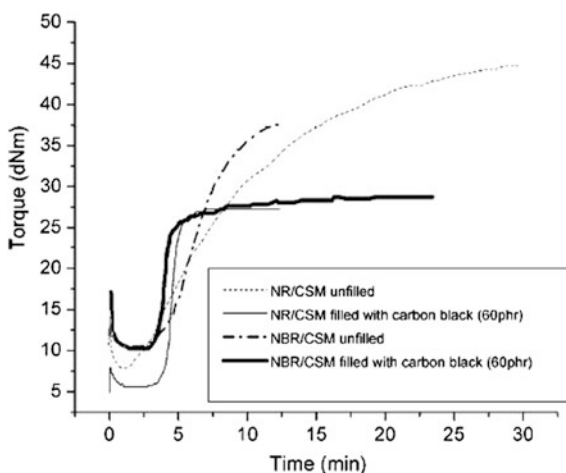
Table 5.14 The obtained data for mechanical properties of cured rubber blends and curing data for compounds with a different content of carbon black

Blend	No	Filler (phr)	Ts (MPa)	Eb (%)	Torque (dNm)		t_{s2} (min)	t_{c90} (min)
					M_{min}	M_{max}		
NR/CSM	1	0	20	573	8.05		2.1	11.3
	2	20	23	529	2.6	25.6	2.3	9.3
	3	40	24	442	3.3	23.6	2.1	8.1
	4	50	25	412	4.1	27.5	1.9	9.7
	5	60	25	343	6.2	32.2	1.8	7.2
	6	80	25	260	6.7	37.3	1.6	8
	7	100	24	220	9.1	40.5	1.6	8.5
NBR/CSM	8	0	14	343	6.8	45.8	8.1	15.2
	9	20	15	381	6.1	48.8	6.3	13.1
	10	40	18	383	6.8	45.7	5.8	13.1
	11	50	20	427	7.1	50.7	4.6	11
	12	60	20	381	7.7	58.6	3.7	5
	13	80	19	373	8.7	52.7	3.3	9.4
	14	100	18	335	9.8	52.7	3.2	9.6

Ts tensile strength; *Eb* elongation at break; t_{s2} scorch time, t_{c90} cure time

5.4.10 Cure Characteristics

The obtained rheometer curves for curing of filled and unfilled rubber blend compounds are given in Fig. 5.12. The cure characteristics of NR/CSM and NBR/CSM rubber blends are summarized in Table 5.14 as the function of the carbon black content together with some other experimental data. The values for curing data depend mainly on the combination of network precursor. The maximum torque, which is a measure of the stiffness of the compound, is directly related to the modulus of the compounds.

The value of the cure time, t_{c90}, is systematically decreased with increasing carbon black content for both rubber blend compounds. The NR/CSM rubber blends have considerably shorter t_{s2} and t_{c90} values than those of carbon black filler of 50 phr or more which resulted again in a noticeable increase in the rate of variation of M100 value with respect to the irradiation dose. These results may be attributed not only to the radiation-induced cross-linking, as well as different interphase linking, but also to the role played by the carbon black filler as a separate phase. In this respect and under a limited extension of 100 % elongation, the carbon black filler would be expected to exist predominantly in its "structure" state, particles aggregated solid and separate form [36]. The effective contribution to the M100 value of vulcanized composites from this solid phase of the filler would then be expected, when taking into consideration that the tensile modulus parameter is an additive in character. The obtained results are in accordance

Fig. 5.13 The effect of the radiation dose on the modulus of NR/CSM blend reinforced with a different content of carbon black
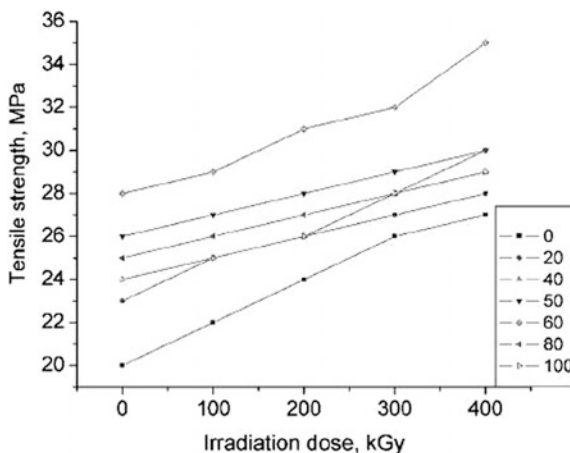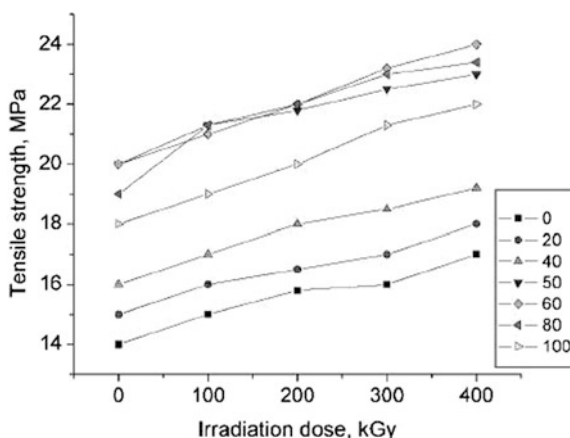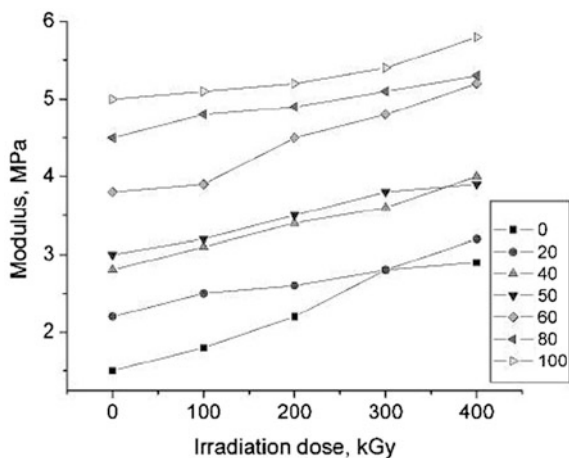

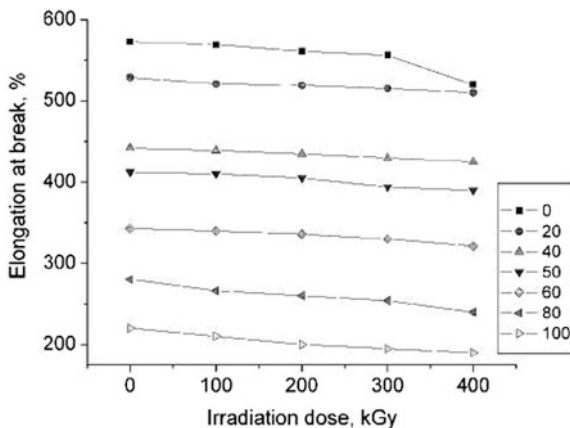**Fig. 5.14** The effect of the radiation dose on the modulus of NBR/CSM blend reinforced with a different content of carbon black

with the comparable results reported before for other rubber composites [37] (Figs. 5.13, 5.14, 5.15, and 5.16).

The variation of the values of elongation at break percent, Eb %, as a function of irradiation dose for unloaded and carbon black-loaded NR/CSM and NBR/CSM blends is depicted in Figs. 5.17 and 5.18, respectively. As expected, the values of Eb for both reinforced blends decrease with increasing irradiation dose. This systematic decrease in Eb values may be attributed to the induced cross-linking by gamma irradiation. On the other hand, the Eb values decreased with the increase in the carbon black filler loading. This reduction is due to stiffening of the matrix by carbon black filler particles [38]. In fact, with any further increase in filler loading, the molecular mobility decreased due to the formation of a physical bonding between the filler particles and the rubber chain. The decrease of Eb values for
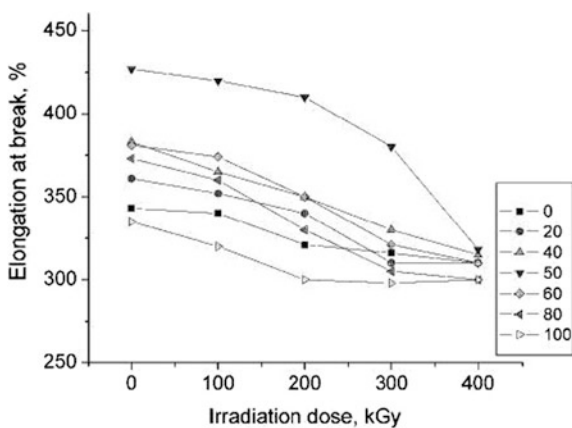
Fig. 5.15 The effect of the radiation dose on the modulus of NR/CSM blend reinforced with a different content of carbon black

Fig. 5.16 The effect of the radiation dose on the modulus of NBR/CSM blend reinforced with a different content of carbon black
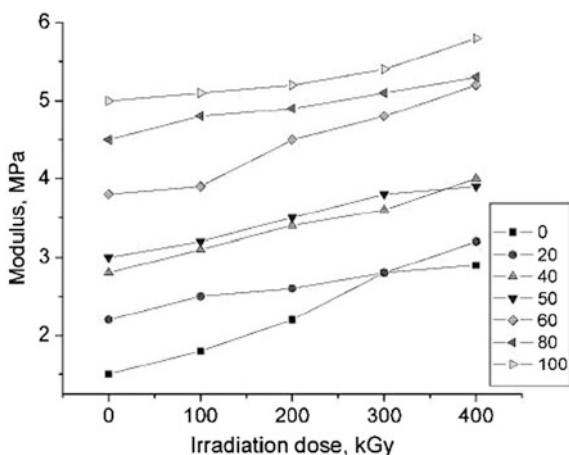
blends loaded with the increasing radiation dose may be explained as an additional bonding between the filler and the rubber due to the large number of free radicals formed under radiation. Therefore, an increased radical recombination is likely to generate strong chemical linkage with an increase of the irradiation dose.

The changes of hardness of loaded and unloaded NR/CSM and NBR/CSM rubber blends as a function of the radiation dose are illustrated in Figs. 5.19 and 5.20, respectively. Also, the data for loaded rubber without irradiation were introduced in the same figure for comparison. It may be observed that the values of hardness of the latter composition have increased effectively with increasing degree of loading with the filler. A similar behavior has been attained for the

Fig. 5.17 The effect of the radiation dose on the elongation at break of NR/CSM blend reinforced with a different content of carbon black

Fig. 5.18 The effect of the radiation dose on the elongation at break of NBR/CSM blend reinforced with a different content of carbon black

Fig. 5.19 The effect of the radiation dose on the hardness of NR/CSM blend reinforced with a different content of carbon black
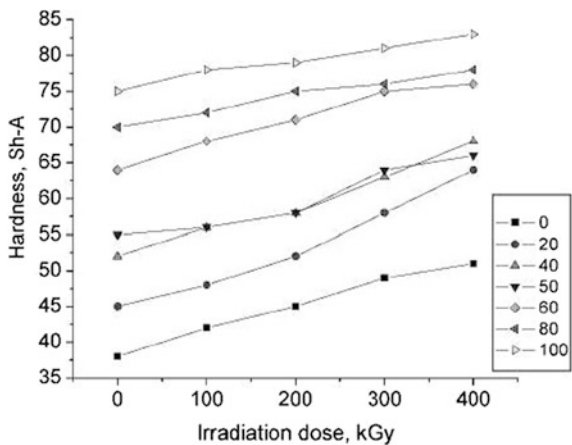
Fig. 5.20 The effect of the radiation dose on the hardness of NBR/CSM blend reinforced with a different content of carbon black
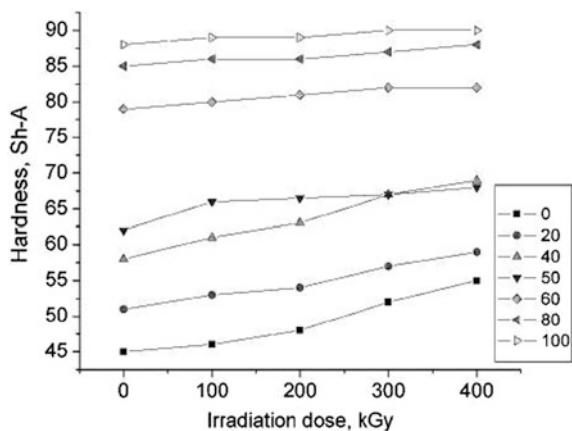
radiation-vulcanized composites when comparing its hardness values at the same irradiation dose. On the other hand, a comparatively limited increase has been attained in the value of hardness for one and the same composition, whether loaded or unloaded, with increasing irradiation dose from 100 to 400 kGy. These data indicate clearly that the contribution to hardness values from the radiation-induced cross-linking that has taken place in the totally amorphous rubber matrix of NBR/CSM blend is a limited one. On the other hand, the main contribution to the hardness value is affiliated with the occurrence of the filler in its aggregated solid and distinct phases, that is, its "structured" form as mentioned before.

Fig. 5.21 SEM of radiated NR/CSM rubber blend filled with carbon black (60 phr)
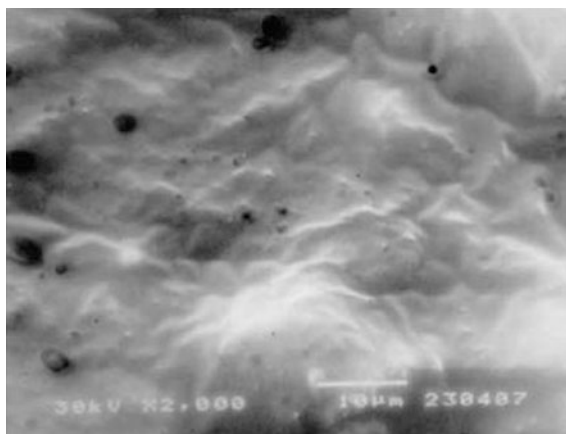
Fig. 5.22 SEM of irradiated
NBR/CSM rubber blend filled
with carbon black (60 phr)
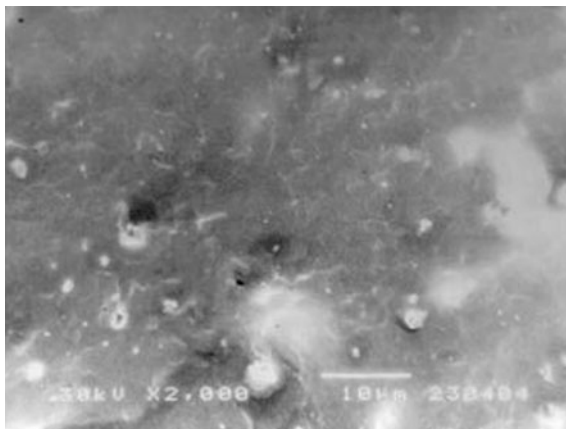
## 5.4.11 Electron Scanning Microscopy

SEM micrographs of fractured surfaces for NR/CSM and NBR/CSM rubber blends
filled with 60 phr are shown in Figs. 5.21 and 5.22, respectively. The formation of
small micro-craters was observed in NBR/CSM rubber blends. A detachment of
small micro-craters from the fractured surface is a result of poor polymer–filler
adhesion. A comparatively good polymer–filler interaction with carbon black and
NR/CSM blend increases the resistance to fracture [39]. Filler distribution in the
blend affects the properties of the obtained elastomeric materials.

5.4.12 FTIR Spectra Measurements

Gamma radiation leads to significant changes in the FTIR spectra of carbon
black-reinforced elastomers based on NR/CSM (Fig. 5.23a, b) and NBR/CSM
(Fig. 5.24a, b) and rubber blend. The broad increase in absorption can be found in
C=O, O–H, and C–O stretching vibration domains for both blends. Significant
changes appeared in the region of conjugated double bonds, too. Several oxidation
products contribute to band at the hydroxyl region, i.e., alcohols (band at 1028–
1075 cm^{-1}), ethers and small amounts of lactones, anhydrides, esters, and car-
boxylic acids. Due to the formation of oxidation products, the bands related to CH_2,
CH_3, =C–H, and C=C vibrations decrease. CH_2 deformation band at 1458 cm^{-1},
CH_3 asymmetric deformation at 1372 cm^{-1}, and =C–H wagging at 831 cm^{-1} show
a significant increase in the spectra of irradiation reinforced rubber blend.

A decrease in absorption at 1660 cm^{-1} is related to the loss of C=C bonds in 1,4-
cis units. 1,4-*cis* units also absorb at 831 cm^{-1}. Beside the oxidation of C=C bonds
in 1,4-cis units, cis-trans isomerization can take place. The band at 2956 cm^{-1}

Fig. 5.23 FTIR spectra
(**a**, **b**) of elastomers aged
under different doses for
NR/CSM rubber blend filled
with carbon black (60 phr)
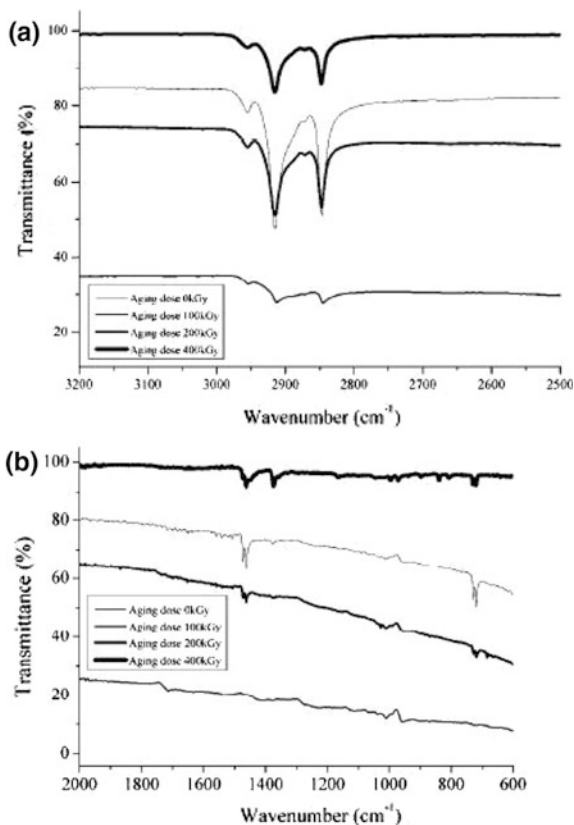
related to methyl groups decreases, especially at the highest doses 200, 300, and
400 kGy. Researchers in the field elastomers based on polyisoprene, acrylonitrile,
and chlorosulfonated polyethylene rubbers [40] did not report the appearance of
new bands related to these processes in the conjugated double-bond region of
radiated NR/CSM and NBR/CSM FTIR spectra. In thermally degraded NR/CSM
and NBR/CSM rubber blends, there have been identified dipentene, two isomeric
forms of dimethylvinylcyclohexene, isoprene, and some aromatic compounds that
formed via the Diels–Alder reactions. Coran [41] reported that during thermal
degradation of 1,4-*cis*-polyisoprene, the chains with conjugated C=C bonds are also
formed. Changes corresponding to similar processes are also present in the region
$1620–1450$ cm^{-1} of the irradiated polyisoprene and acrylonitrile spectra, where no
oxidation product absorbs. Polyenes and polyenals show several bands in the 1500–
1650 cm^{-1} range. Benzene C=C stretching vibration bands are located between
1600 and 1450 cm^{-1}; hydrogen bond can cause the reduction of the stretching
vibration frequency. The subtraction spectra reveal the occurrence of the broad
band with a significant increase in absorption at 1470 cm^{-1}. This band can be
assigned to aromates and shorter polyene structures. Absorption at 1470 cm^{-1}

Fig. 5.24 FTIR spectra
(**a**, **b**) of elastomers aged
under different doses for
NBR/CSM rubber blend filled
with carbon black (60 phr)
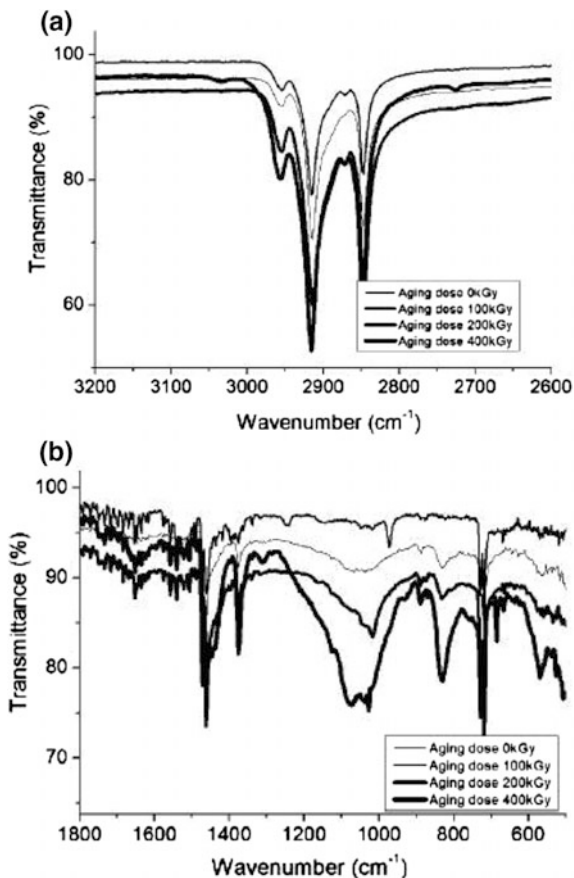
remains the same (the maximum is slightly shifted to higher wave numbers) for the highest doses, and absorption at 1461 cm–1 was lower in the case of the sample irradiated with the highest dose (Figs. 5.23 and 5.24). It implies that formed species are a subject of consecutive reactions. It can be concluded that radiation induces serious changes in NR/CSM and NBR/CSM rubber blends' backbone chain scissions and various consecutive reactions take place. These changes are noticeable in the 1470–1450 cm^{-1} region that indicates the occurrence of the polyene sequences and aromatic rings. Contrary to the chain scission reactions [42], the formation of cross-links is difficult to detect by using IR spectroscopy due to the overlap of many bands in the region of C–C stretching vibrations. Doses exceeding 200, 300, and 400 kGy caused serious modification to the polymer structures.

The influence of carbon black (with an average particle size of 40 nm) on gamma radiation resistance of rubber blends was investigated. The mechanical properties of elastomer depend mainly on the carbon black loading. Tensile strength, modulus at 100 % elongation, and hardness were increased with

increasing radiation dose, as well as carbon black loading, but the elongation at break values decreases with increasing radiation dose and carbon black content. The FTIR spectra of aged samples confirmed the formation of various oxidation products, i.e., alcohols, ethers and small amounts of lactones, anhydrides, esters, and carboxylic acids during radiation. Significant changes in spectra are induced by chain scission which was registered in the 1620–1450 cm^{-1} region. The formation of shorter polyene sequences and aromatic rings is assumed. The radiation doses lower than 100 kGy influenced only small changes in the rubber macromolecular structure if we consider the development of the bands in carbonyl and conjugated C=C bond regions. On the other hand, 200, 300, and 400 kGy doses caused a serious chemical modification to the prepared rubber blend samples.

5.4.13   CSM/IIR and CSM/CIIR Rubber Blend

The incorporation of CSM in CSM/IIR and CSM/CIIR blends increases the scorch time, t_{s2}, and cure time, t_{c90}. At a similar CSM content, the CSM/CIIR blend exhibits shorter scorch time t_{s2} and cure time t_{c90} than the CSM/IIR blend. The incorporation of CSM in the CSM/CIIR blend also increases the maximum torque (M_h) and torque difference $(M_h - M_l)$. However, for the CSM/IIR blend, the maximum torque and torque difference decrease with the incorporation of CSM, an observation which is attributed to the maldistribution of cross-link between the two rubber phases. M100 and M300 increase with increasing CSM content in both blends. The former increase is attributed to the enhancing effect of CSM, and the latter increase is associated with strain-induced crystallization of the respective rubbers. Tensile strength and elongation at break of the blends decrease gradually with CSM content, an observation which is ascribed to the decreasing effect of strain-induced crystallization of IIR and CIIR as CSM content is increased in the respective blends. The cross-linking density is found to slightly change with an increase in the concentration of the CSM rubber in CSM/CIIR and CSM/IIR rubber blends. Higher cross-linking density is obtained for CSM/CIIR rubber blends. The micrograph of CSM/CIIR exhibits that the composite's surface is rough with many tear lines and branching indicates the higher tensile strength and a weak interaction between CSM and CIIR rubbers.

Figures 5.25 and 5.26 show the effect of CSM content on the scorch time t_{s2} and cure time, t_{c90}, of the CSM/IIR and CSM/CIIR rubber blends. It can be seen that the t_{s2} and t_{c90} of these blends increase with increasing CSM content. CIIR and CSM are polar rubber. As the content of CSM in the blends is increased, the curative agent, i.e., sulfur, becomes more soluble in CSM and CIIR compared to IIR. Consequently, the curing rate of the blend increases with increasing content of CSM. Researches [43–45] reported that for blends of two rubbers with similar polarity, distribution of cross-links can be equal through phases. It can be seen also in Figs. 5.25 and 5.26 that at a similar CSM content, t_{s2} and t_{c90} of CSM/CIIR blend are shorter than those of CSM/IIR blend. The effect of CSM content on the maximum torque

Fig. 5.25 Variation of scorch
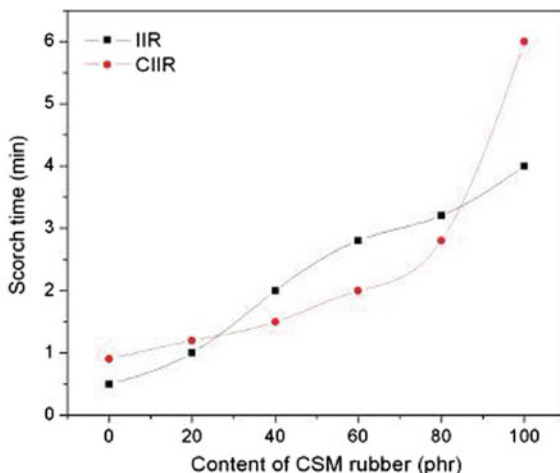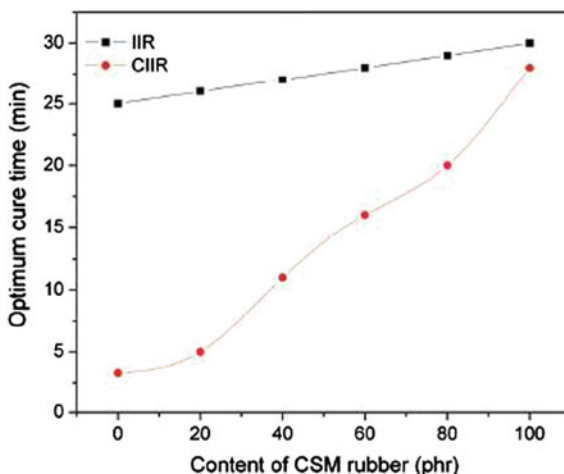time t_{s2} with CSM content at
160 °C for CSM/IIR and
CSM/CIIR blends

Fig. 5.26 Variation of cure
time t_{c90} with CSM content at
160 °C for CSM/IIR and
CSM/CIIR blends

(M_h) is shown in Fig. 5.27. It can be seen that the M_h increases with increasing CSM
content in the CSM/CIIR blend. Figure 5.27 also shows that above 40 phr of CSM,
M_h of CSM/CIIR blends has higher values than CSM/IIR blend as a result of the
miscibility presence between CSM and CIIR rubber. The relationship between the
torque difference, $\Delta M = M_h - M_l$ (max. torque − min. torque), and content of CSM
is shown in Fig. 5.24. It is known that the torque difference indirectly relates to the
cross-linking density of the blends [46]. This figure clearly shows that CSM/CIIR
blend is a more compatible blend than CSM/IIR blend. The decreasing torque dif-
ference for CSM/IIR indicates that a distribution of cross-link occurred which results
in an over-cross-linked phase and a poorly cross-linked one.

Fig. 5.27 Maximum torque M_h versus CSM content at 160 °C for CSM/IIR and CSM/CIIR rubber blend
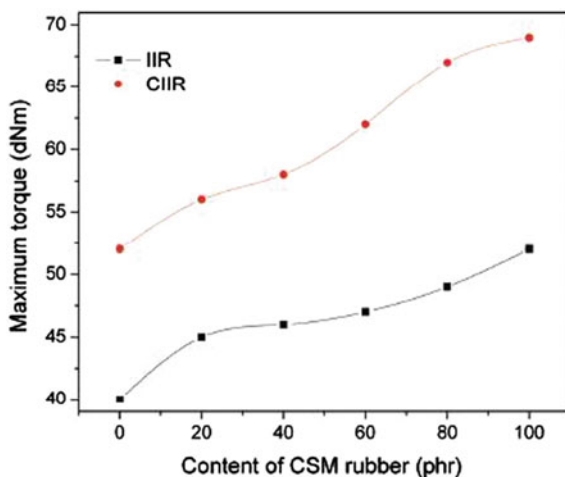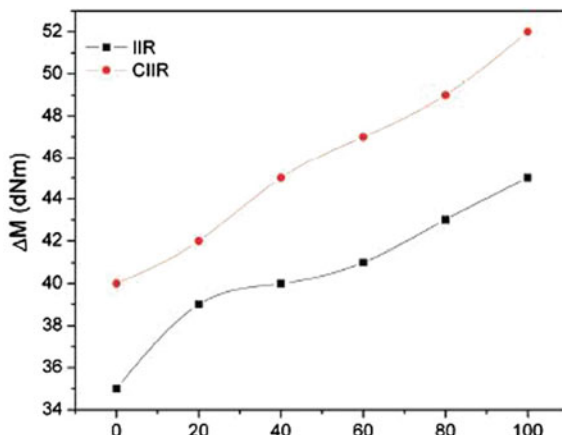

Fig. 5.28 Torque difference $(M_h - M_l)$ versus CSM content at 160 °C for CSM/IIR and CSM/CIIR blends

Again at a similar CSM content, CSM/CIIR blend exhibits higher $M_h - M_l$ than CSM/IIR blend. Markovic [47] reported that with normal sulfur-vulcanizing systems, the efficiency of CIIR vulcanization seemed to be improved. The isolated double bonds in CIIR inhibit the formation of intramolecular sulfide links, thus resulting in the increase of the cross-linking rate (Fig. 5.28).

Fig. 5.29 Modulus at 100 %
elongation versus CSM
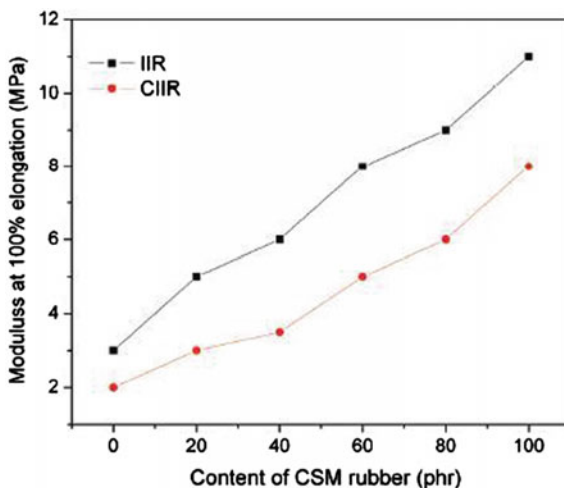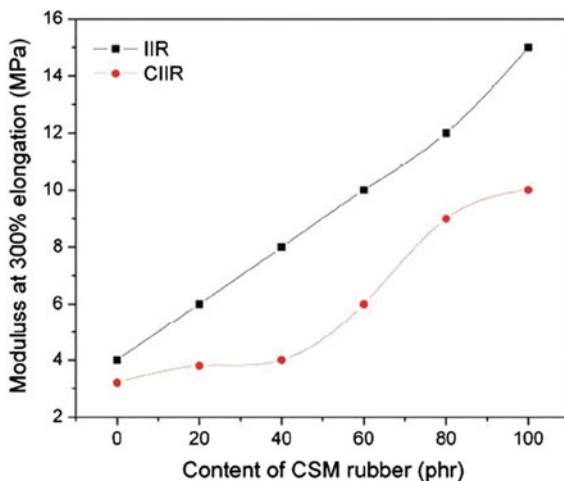content at 160 °C for
CSM/IIR and CSM/CIIR
rubber blend

Fig. 5.30 Variation of M300
with CSM content in the
blends

5.4.14 Mechanical Properties

Figure 5.29 shows the variation of M100 with CSM content in the two CSM/IIR
and CSM/CIIR rubber blends. It is obvious that as the percent of CSM increases,
M100 also increases correspondingly.

This means that the incorporation of CSM in the blend would enhance
cross-linking as M100 is a measure of degree of cross-linking. CSM/CIIR blend
gives a higher M100 value than the CSM/IIR blends. This observation may be
attributed to greater enhancement effect of CSM on CIIR. In fact, the cross-linking
density is increased for both blends. As in the case of CSM/IIR blend, the lower

Fig. 5.31 Variation of tensile strength with CSM content in the blends
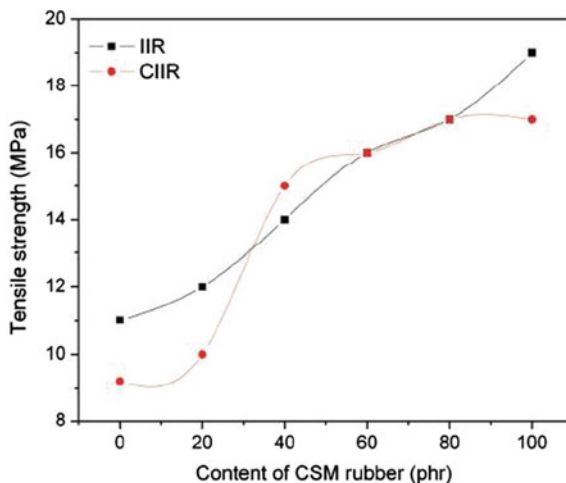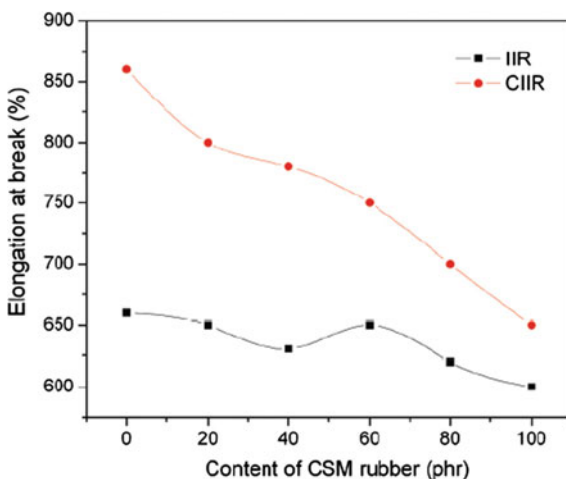

Fig. 5.32 Variation of elongation at break with CSM content in the blends

M100 is attributed to the non-enhancement effect of CSM which is a polar polymer compared to IIR, a nonpolar rubber. Thus, the CSM/IIR blend has a lower cross-linking density than CSM/CIIR blends. The variation of M300 with CSM content is presented in Fig. 5.30. In this case, CSM/IIR blend consistently shows a higher M300 than CIIR blends.

The increase of M300 values indicates that CSM reinforces IIR and CIIR blends: The degree of reinforcement is greatest in IIR, followed by CIIR as the degree of crystallization decreases with increasing % of halogenated. Figure 5.11 shows the dependence of tensile strength of the two rubber blends on CSM content. Again, IIR blend consistently indicates a higher tensile strength than the CIIR blend as observed for M300. However, in this case, tensile strength decreases gradually with

increasing CSM content for all the blends studied. This observation is associated with decreasing effect of strain-induced crystallization as CSM content is increased. As discussed earlier in M300, IIR exhibits the greatest strain-induced crystallization, followed by CIIR. This sequence of decreasing crystallization is reflected by the decreasing value of tensile strength for the respective single-component rubbers [48]. In the case of CSM, it has the lower tensile strength due to the non-crystallizable nature of the rubber. Figure 5.31 also shows that for CSM content greater than 60 phr, greater drop in tensile strength for the blends is observed. This finding may be ascribed to the dominant effect of CSM at higher loading of CSM.

The effect of CSM on elongation at break for CSM/IIR and CSM/CIIR rubber blends is shown in Fig. 5.32. The effect, in fact, is very similar to that of tensile strength; that is, elongation at break decreases gradually with increasing CSM content. Owing to the higher strength of IIR, its blend gives a much higher elongation at break compared to CIIR blend. For the single-component CSM, its elongation at break is the lowest among the rubbers studied due to the non-crystallizable property of CSM.

5.4.15 Swelling Properties

Some calculated data for the "relative" cross-linking density values, v, obtained from the swelling measurements for rubber blends are given in Table 5.15. The cross-linking density is found to slightly change with an increase in the concentration of the CSM rubber in CSM/CIIR and CSM/IIR rubber blends. Higher cross-linking density is obtained for CSM/CIIR rubber blends; this is because of the restriction of swelling due to the similar (polar) nature of rubbers and formation of

Table 5.15 The data of the cross-linking density reciprocal swelling ratio ($1/Q$) volume fraction of CSM/CIIR and CSM/IIR rubber blends in swollen gel (Φ_p), molecular weight between cross-link (M_c) and Flory Huggins parameter (χ) from swelling measurements

| Sample	$v \times 10^3$ (mol dm^{-3})	Qr	$1/Q$	M_c (gmol^{-1})	χ
CSM/IIR/CIIR (100/0/0)	710	0.32	0.48	750	0.42
CSM/IIR/CIIR (80/20/0)	795	0.33	0.41	762	0.42
CSM/IIR/CIIR (60/40/0)	800	0.33	0.47	778	0.41
CSM/IIR/CIIR (40/60/0)	810	0.34	0.47	780	0.41
CSM/IIR/CIIR (20/80/0)	830	0.34	0.47	790	0.4
CSM/IIR/CIIR (0/100/0)	832	0.34	0.47	790	0.41
CSM/IIR/CIIR (80/20/0)	812	0.33	0.47	791	0.42
CSM/IIR/CIIR (60/40/0)	824	0.33	0.47	770	0.42
CSM/IIR/CIIR (40/60/0)	831	0.34	0.47	814	0.41
CSM/IIR/CIIR (20/8/0)	847	0.34	0.47	831	0.41
CSM/IIR/CIIR (100/0/0)	850	0.34	0.47	821	0.41
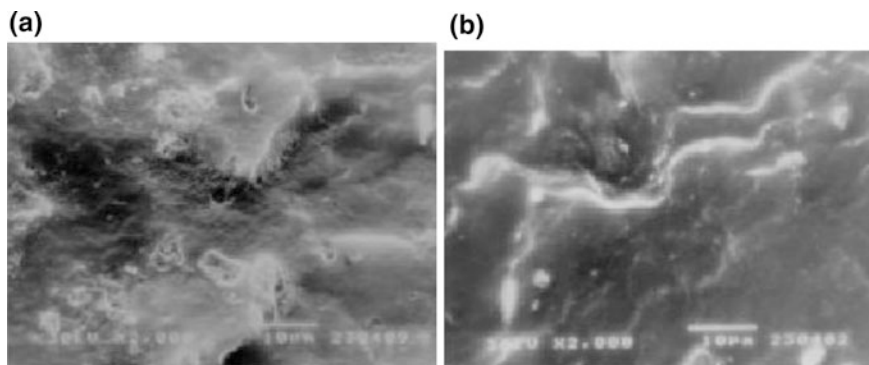
Fig. 5.33 SEM micrograph of CSM/IIR (60/40) (**a**) and CSM/CNR (60/40) rubber blends (**b**)

new cross-links according to free sulfur and residues of curatives react with rubbers, which causes an increase in Φ_p and increases the cross-linking density. Thus, the observed tensile strength variation can be exactly correlated with the variation of v from swelling studies. In swelling studies of these samples, cross-links are flexible to penetrate, but as the loading of CSM increases, they restrict the swelling. The swelling ratio, $1/Q$, calculated using Eq. (5.1) is found to increase (Table 5.15).

5.4.16 Morphological Study

In Fig. 5.33a, b, the SEM photomicrograph of CSM/IIR and CSM/CIIR (60/40) rubber blends at 2000× magnification is shown. The micrograph of CSM/CIIR (Fig. 5.33b) exhibits that the composite's surface is rough with many tear lines and branching.

This type of failure indicates the higher tensile strength and a weak interaction between CSM and CIIR rubbers.

5.5 Recent Advances on Chlorosulfonated Rubber Nano-blends

Thermostability and surface morphology of nano- and micro-filled NBR/CSM and CR/CSM rubber blends. Cross-linked NBR/CSM and CR/CSM rubber systems with a mass ratio of 50:50 (Table 5.5) have good weather resistance, color stability, high ozone resistance, and high extension values.

Table 5.16 Glass transition temperature (T_g) for 10 and 30 % weight loss and other characteristic temperatures of unfilled and nano- and micro-particle-sized SiO_2-filled NBR/CSM and CR/CSM cross-linked systems

Compounds	T_{max} (°C)	$T_{10\%}$ (°C)	$T_{30\%}$ (°C)	T_{end} (°C)	M_{rest} (%)	T_g (°C)
NBR	434	403	427	707	3.37	−22
CSM	348	319	354	655	25.4	−37
NBR:CSM (50:50)	449	312	429	472	3.8	−20
NBR:CSM + SiO_2 (15 nm)	452	303	424	486	33.1	−27
NBR:CSM + SiO_2 (28 μm)	450	296	425	485	38.6	−28
CR	282	283	300	590	28.9	−39
CR:CSM (50:50)	466	252	326	537	16.9	−38
CR:CSM + SiO_2 (15 nm)	463	257	349	605	30.3	−40
CR:CSM + SiO_2 (28 μm)	465	259	361	565	32.6	−45

5.5.1 Thermal Stability

The thermal stability analysis was based on the temperature for certain weight losses, namely 10 and 30%, and the rate of weight loss changes as a function of temperature (first derivative of the dynamic TG curve) i.e., the initial and overall shapes. The first corresponds to the partial degradation of the sample, and the second is the result of complete thermal decomposition. The samples could be characterized by the position of the decomposition peaks and their size, the difference being the result of the different influence of their structure and the differences in the degradation processes. The data for the 10 and 30 % weight loss temperatures are given in Table 5.16.

From the values of the temperatures at 10 % weight loss and T end, it can be seen that the nanoparticle-sized SiO_2-filled NBR/CSM cross-linked systems (303, 486 °C) are more stable than the micro-particle-sized SiO_2-filled NBR/CSM cross-linked systems (296, 485 °C). In the CR/CSM cross-linked systems, the temperature values at 10 % weight loss show little difference in the thermostability between the micro-particle-sized SiO_2 and the nanoparticle-sized SiO_2-filled cross-linked systems. In the next step (30 % weight loss), the micro-filled cross-linked system had more stability than the nano-filled cross-linked system. Among the most important factors that can influence the initial TG behavior are the strength of the bonds in the main CR/CSM and NBR/CSM polymer chains and the bonds with SiO_2. The single glass transition temperature for the NBR/CSM and CR/CSM cross-linked systems indicates that NBR, CSM, and CR are compatible. The higher values of the glass transition temperatures for the nano- than for the micro-filled cross-linked systems indicate that nano-filled cross-linking systems have greater number of SiO–C links than micro-filled cross-linking systems and more stability.

5.6 Industrial Values and Applications

In recent years, economic, technological, and other regulatory pressures have gradually narrowed the further development of new chemical varieties of polymers [49, 50]. A blend can offer a set of properties that may give it the potential of entering application areas not possible with either of the polymer comprising the blends. Among the authors investigating rubber blends, Baker [51] reported that replacement of polychloroprene by a 20/80 natural rubber/neoprene GRT blend could be accessible for many applications where neoprene GRT is used; Patra and Das [52] studied the flame retardancy and heat shrinkability of polyolefin/elastomer blends. The blending together of natural rubber (NR) and chlorosulfonated polyethylene rubber (CSM) is intended to produce a vulcanizate with the best properties from each component, i.e., the good strength properties of NR and the good weather resistance, color stability, and high extension values of CSM.

5.6.1 CSM/SMR 20 CV and CSM/Pergut S 40 Rubber Blends

The Mooney scorch time, t_5, of CSM/SMR 20 CV and CSM/Pergut S 40 blends decreases with increasing SMR20 CV and Pergut S 40 content in the blends. The reduction is more pronounced at lower temperatures, i.e., below 130 °C. For CSM/SMR 20 CV blend, the cure index shows a maximum at 20 phr of SMR 20 CV in the blend at lower vulcanization temperature, an observation which is attributed to the incompatibility between CSM and SMR 20 CV and the faster cure rates of the latter. In the case of CSM/Pergut S 40 blends, the cure rate virtually decreases with increasing Pergut S 40 content, as a result of the better compatibility between CSM and Pergut S 40, both of which are polar in nature. For temperature greater than 140 °C, the cure index for both blend systems exhibits less dependence on the blend ratio due to the availability of thermal energy to overcome the

Fig. 5.34 Variation of the Mooney scorch time with blend ratio of SMR 20 CV (phr) in the CSM/SMR 20 CV blend for various vulcanization temperatures
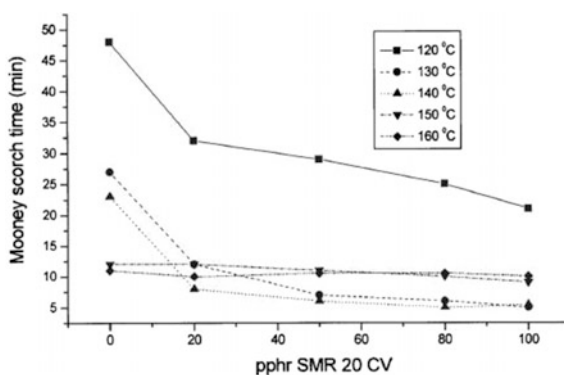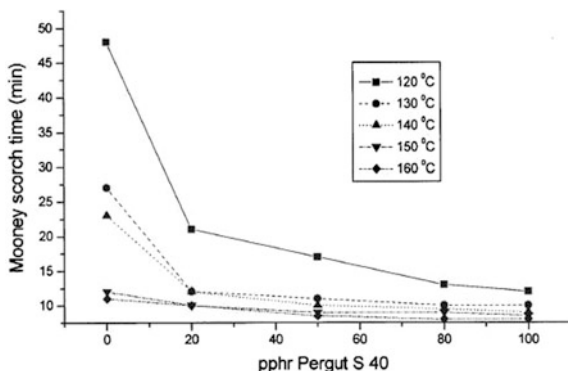
Fig. 5.35 Variation of the Mooney scorch time with blend ratio of Pergut S40 (phr) in the CSM/Pergut S40 (phr) blend for various vulcanization temperatures

activation energy of vulcanization. Based on the morphological investigations, the fracture surfaces of CSM/SMR 20 CV (80:20) rubber blends are less homogeneous than those of CSM/Pergut S 40 (80:20).

Scorch Time

The variation of the Mooney scorch time, t_5, of the CSM/SMR 20 CV and CSM/Pergut S 40 blends with a blend ratio of SMR 20 CV and Pergut S 40 is shown in Figs. 5.34 and 5.35, respectively.

It can be seen that the t_5 of the blends decreases with increasing SMR 20 CV and Pergut S 40 content. CSM is a polar rubber. As the content of CSM in the blends decreases, the curing agents, i.e., sulfur, magnesium oxide, and tetramethylthiuram disulfide, become more soluble in the SMR 20 CV and Pergut S 40 than in the CSM. Consequently, the cure rate of the blend increases with decreasing content of CSM. According to Lewan [53], for blends with two rubbers differing in polarity, such as SMR 20 CV or Pergut S 40 with CMS, a distribution of cross-links can arise through

Fig. 5.36 Variation of the Mooney scorch time at 120 °C with the ratio of Pergut S40 and SMR CV60 (phr) in the CSM/SMR 20 CV and CSM/Pergut S40 rubber blend
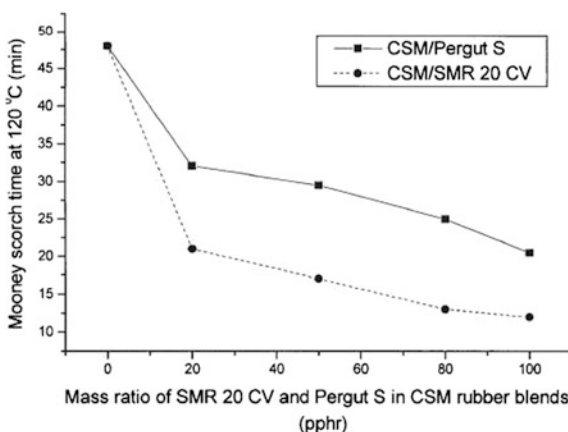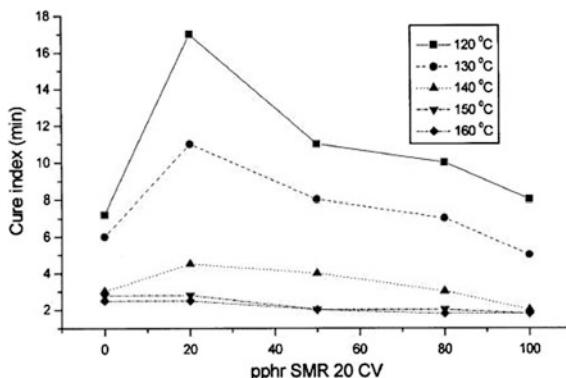
Fig. 5.37 Variation of the cure index blend ratio of SMR 20 CV (phr) in the CSM/SMR 20 CV rubber blend for various vulcanization temperatures

preferential solubility of the curing agents and vulcanization intermediates. Both figures also indicate that the reduction of t_5 with a blend ratio of SMR 20 CV and Pergut S 40 is more pronounced at temperatures lower than 130 °C. At higher temperatures, i.e., higher than 140 °C, t_5 does not show a significant dependence on the blend ratio because enough thermal energy is available to overcome the activation energy of vulcanization. A comparison of t_5 for CSM/SMR 20 CV and CSM/Pergut S 40 blends at 120 °C is shown in Fig. 5.36. It can be seen that with a similar blend ratio, the t_5 of the CSM/SMR 20 CV blend is shorter than that of the CSM/Pergut S 40 rubber blend. According to Poh and Wong [54], more activated precursors to cross-links are formed which accelerate the vulcanization process.

Cure Index

The dependence of cure index of the CSM/SMR 20 CV blend on the blend ratio of SMR 20 CV for the various temperatures investigated in this study is shown in Fig. 5.37. For temperatures lower than 140 °C, the cure index is significantly dependent on the blend ratio of SMR 20 CV. It passes through a maximum at 20 phr of SMR 20 CV in the blend. This observation is attributed to the incompatibility between CSM (a polar rubber) and SMR 20 CV (a nonpolar rubber), the respective solubility parameters of which are 9.5 and 8.1.11 [55]. Also, owing to the higher unsaturation in SMR 20 CV, it cures faster than CSM, resulting in uneven vulcanization of the blend. For instance, at 120 °C, the cure index of CSM and that of SMR 20 CV are 7.2 and 8 min, respectively. As the SMR 20 CV content in the blend is increased from 0 to 20 phr, more sulfur reacts with the SMR20 CV rubber than with CSM. This means that less sulfur and magnesium oxide are available for the vulcanization of CSM, which is the dominant rubber component in the blend. However, beyond 20 phr of SMR 20 CV, the role of SMR 20 CV becomes more significant and results in a drop of the cure index of the blend. For the temperatures greater than 140 °C, the cure index shows less dependence on the blend ratio of SMR 20 CV, a phenomenon that is associated with the increase in cure rates for

Fig. 5.38 Variation of the cure index blend ratio of Pergut S (phr) in the CSM/Pergut S rubber blend for various vulcanization temperatures
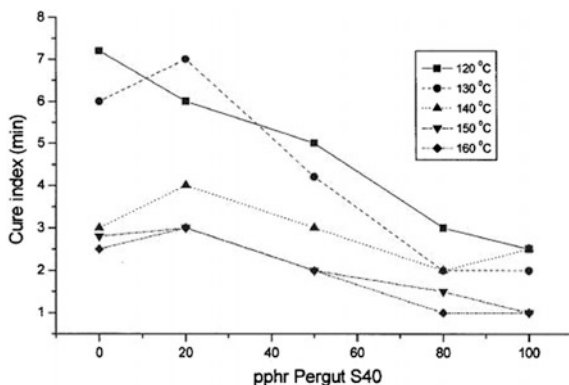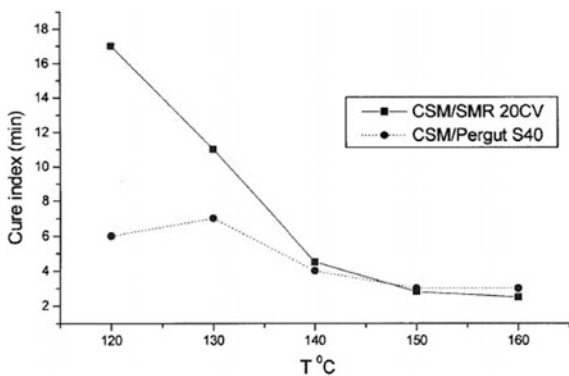

Fig. 5.39 Temperature dependence of the cure index at 20 phr of Pergut S40 and SMR CV60 (phr) in the CSM/SMR 20 CV and CSM/Pergut S40 rubber blend

both rubbers resulting from an ample supply of thermal energy to overcome the activation of vulcanization for both rubbers, i.e., even vulcanization of the blend is obtained. In fact, above 150 °C, the cure index is almost independent of the blend ratio of SMR 20 CV.

The effect of blend ratio of Pergut S 40 on the cure index of CSM/Pergut S 40 blend is shown in Fig. 5.38. Generally, a gradual drop of cure index is observed as the phr of Pergut S 40 is increased, although a slight maximum is displayed in some cases. This finding is attributed to the better compatibility between CSM and Pergut S 40, both of which have a polar nature. The respective solubility parameters are 9.5 and 9.2.9 [56] which are closer than the corresponding values for CSM and SMR 20 CV, as discussed earlier. As in the case of the CSM/SMR 20 CV system (Fig. 5.38), the cure index of the blend was less dependent on the blend ratio of Pergut S 40 at higher vulcanization temperature, i.e., greater than 140 °C. Again, this is attributed to the availability of thermal energy to overcome the activation energy of vulcanization.

In order to compare the cure index of both blends, the cure index was plotted against the cure temperature for blends, containing either 20 phr SMR 20 CV or

Pergut S 40 (Fig. 5.39). The cure index decreases with increasing temperature for both blends. The cross-linking of CSM takes place according to a completely different mechanism from those involved in the cross-linking of natural rubber i.e., the activation energy is different.

5.7 Conclusion

Blending of two or more different types of rubber is considered a useful technique for developing materials with properties superior to those of individual constituents or ones which demonstrate useful property combinations. The approach is important especially from a technical point of view. Elastomeric materials based on the chlorosulfonated polyethylene (CSM) rubber nano-blend have a quite good crack resistance, wet grip, and weather resistance. On the other hand, it shows a good resistance to interactions with alcohols as well as strong acids and bases. This type of material also exhibits excellent ultraviolet light and oxygen stability. In addition to applications for glovebox gloves, this rubber has additional uses such as in lining and sheath materials, coatings, and adhesives. CR/CSM rubber blend study illustrates the intrinsic potential of nano-silica particle size as reinforcing filler in elastomeric materials. The nano-silica-filled CR/CSM rubber blends have higher values for cure characteristics than micro-silica particle-sized filled compounds. Nano-silica type activated the vulcanizing process through the promotion of hydrogen sulfide formation and the rupture of S–N linkage when heated with sulfonamides in rubber either in the presence or in the absence of other compounding ingredients. The strong peak from SiO–C at 1070 and 1079 cm^{-1} in the IR spectrum of nano- and micro-silica-filled CR/CSM rubber blend suggested the presence of interaction with silica which leads to increased stability of the filled CR/CSM polymer blends. According to the Kraus equation, it can be observed that the nano-silica-filled CR/CSM rubber blend has higher V_{r0}/V_{rf} values and better rubber filler interactions than micro-silica-filled composites. The higher values of the glass transition temperatures for the nano- than the micro-filled cross-linked systems are indicated by DMA analysis. The density of the nano-silica-filled CR/CSM rubber blends was lower than that of the micro-silica-filled and was transparent at all filler concentration.

For SBR/CSM blends, the addition of filler leads to a significant enhancement in the physical properties if CSM is the major blend constituent. The blends containing CB N339 show higher hardness, tensile strength, and abrasion resistance when compared to the ones containing CB N772. The experimental data indicate that this can be caused by the improvement in the polymer–filler phase bonding which results from the interfacial interaction of functional groups of the polymer and the active sites of the filler surface leading to a higher apparent cross-linking density. As the concentration of CSM in the rubber blend increases, the cure characteristics, such as optimum cure time, scorch time, and induction time at

160 °C, increase for the blends filled with CB N339. The results for the curing behavior are consistent with the mechanical properties of the SBR/CSM blends.

The influence of carbon black (with an average particle size of 40 nm) on gamma radiation resistance of rubber blends was investigated. The mechanical properties of elastomer depend mainly on the carbon black loading. Tensile strength, modulus at 100 % elongation, and hardness were increased with increasing radiation dose, as well as carbon black loading, but the elongation at break values decrease with increasing radiation dose and carbon black content. The FTIR spectra of aged samples confirmed the formation of various oxidation products, i.e., alcohols, ethers and small amounts of lactones, anhydrides, esters, and carboxylic acids during radiation. Significant changes in spectra are induced by chain scission which was registered in the 1620–1450 cm^{-1} region. The formation of shorter polyene sequences and aromatic rings is assumed. The radiation doses lower than 100 kGy influenced only small changes in the rubber macromolecules structure if we consider the development of the bands in carbonyl and conjugated C=C bond regions. On the other hand, 200, 300, and 400 kGy doses caused a serious chemical modification of the prepared rubber blend samples.

The incorporation of CSM in CSM/IIR and CSM/CIIR blends increases the scorch, t_{s2}, and cure time, t_{c90}. At a similar CSM content, the CSM/CIIR blend exhibits shorter scorch time t_{s2} and cure time t_{c90} than the CSM/IIR blend. The incorporation of CSM in the CSM/CIIR blend also increases the maximum torque (M_h) and torque difference ($M_h - M_l$). However, for the CSM/IIR blend, the maximum torque and torque difference decrease with the incorporation of CSM, an observation which is attributed to the maldistribution of cross-link between the two rubber phases. M100 and M300 increase with increasing CSM content in both blends. The former increase is attributed to the enhancing effect of CSM, and the latter increase is associated with strain-induced crystallization of the respective rubbers. Tensile strength and elongation at break of the blends decrease gradually with CSM content, an observation which is ascribed to the decreasing effect of strain-induced crystallization of IIR and CIIR as CSM content is increased in the respective blends. The cross-linking density is found to slightly change with an increase in the concentration of the CSM rubber in CSM/CIIR and CSM/IIR rubber blends. Higher cross-linking density is obtained for CSM/CIIR rubber blends. The micrograph of CSM/CIIR exhibits that the composite's surface is rough with many tear lines and branching indicates the higher tensile strength and a weak interaction between CSM and CIIR rubbers.

Nano-silica filler interacts more with NBR/CSM and CR/CSM polymer matrix than micro-silica, which is the result of the greater contact area of the nano-filler, greater adsorption, and lower mobility of the polymer chains or the filler surface. The higher values of the glass transition temperatures for the nano- than the micro-filled cross-linked systems indicate that the nano-filled cross-linked systems have a larger number of SiO–C links than micro-filled cross-linked systems and hence increased stability. According to morphological investigation, can be concluded: (i) The surface of NBR/CSM polymer blends is more polished than that of CR/CSM polymer blends and without crack; (ii) the presence in both NBR/CSM

and CR/CSM rubber blends with micro-particle size of SiO_2 of rubber balls and some amount of fibrosity in the matrix, voids and crazes, as well as micro-cracks and crystallinity contribute toward failure of the macromolecular network structure. The increased number of cracks and voids in the CR/CSM polymer blends contribute to the earlier loss of physical and mechanical properties, compared to the NBR/CSM polymer blends.

The Mooney scorch time, t_5, of CSM/SMR 20 CV and CSM/Pergut S 40 blends decreases with increasing SMR20 CV and Pergut S 40 content in the blends. The reduction is more pronounced at lower temperatures, i.e., below 130 °C. For CSM/SMR 20 CV blend, the cure index shows a maximum at 20 phr of SMR 20 CV in the blend at lower vulcanization temperature, an observation which is attributed to the incompatibility between CSM and SMR 20 CV and the faster cure rates of the latter. In the case of CSM/Pergut S 40 blends, the cure rate virtually decreases with increasing Pergut S 40 content, as a result of the better compatibility between CSM and Pergut S 40, both of which are polar in nature. For temperature greater than 140 °C, the cure index for both blend systems exhibits less dependence on the blend ratio due to the availability of thermal energy to overcome the activation energy of vulcanization. Based on the morphological investigations, the fracture surfaces of CSM/SMR 20 CV (80:20) rubber blends are less homogeneous than those of CSM/Pergut S 40 (80:20).

References

1. Marković G, Samaržija-Jovanović S, Jovanović V, Marinović-Cincović M, Budinski-Simendić J (2009) Chem Ind Chem Eng Q 15(4):291–298
2. Omran AM, Youssef AM, Ahmed MM, Abdel-Bary EM (2010) Kautch Gummi Kunst 6:197–202
3. Wu S (1985) Polymer 26(12):1855–1863
4. Marković G, Samaržija-Jovanović S, Jovanović V, Marinović-Cincović M (2010) J Therm Anal Calorim 100:881–888
5. Essawy H, El-Nashar D (2004) Polym Testing 23(7):803–807
6. Marković G, Radovanović B, Marinović-Cincović M, Budinski-Simendić J (2006) Kautch Gummi Kunst 5:251–255
7. Voet A (1980) J Polym Sci 15:327–373
8. Flory PJ (1946) Ind Eng Chem 38(4):417–436
9. Roychoudhury A, De PP (1997) J Appl Polym Sci 63(13):1761–1768
10. Zhang L, Wang Y, Wang Y, Sui Y, Yu D (2000) J Appl Polym Sci 78(11):1873–1878
11. Mostafa A, Abouel-Kasem A, Bayoumi MR, El-Sebaie MG (2009) Mater Des 30:1561–1568
12. Liu Q, Zhang Y, Xu H (2008) Appl Clay Sci 42:232–237
13. Das A, Costa FR, Udo W, Heinrich G (2008) Eur Polym J. 44:3456–3465
14. Odlyhal M, Cohen NS, Foster GM, Aliev A, Verdonck E, Grandy D (2003) J Therm Anal Calorim 71:939–950

15. Furtado CRG, Leblanc JL, Nunes RCR (1999) Eur Polym J 35:1319
16. Yatsuyanagi F, Suzuki N, Ito M, Kaidou HE (2001) Polymer 42:9523
17. Akovali G, Ulkem I (1999) Polymer 40:7417
18. Mann DG, Evans KM (2007) Molecular genetics and the neglected art of diatomics. In: Brodie J, Lewis J (eds) Unravelling the algae—the past, present and future of algal systematics. CRC Press, Boca Raton (Florida)
19. Williams DM, Kociolek JP (2007) Eur J Phycol 42:313–319
20. Markovic GS, Veljkovic O, Marinovic-Cincovic MT, Jovanovic V, Samarzija-Jovanovic S, Budinski-Simendic JK (2013) Compos Part B Eng 45 br. 1, str. 178–184
21. Stojčeva-Radovanović B, Marković GS, Marinović-Cincović MT, Babić D , Nedeljković JM (2002) Hemijska industrija 56(10):415–421. doi:10.2298/HEMIND0210415S
22. Markovic GS, Marinovic-Cincovic MT, Jovanovic V, Samarzija-Jovanovic S, Budinski-Simendic J (2014) Chapter: Non-linear. Non-linear viscoelasticity of rubber composites and nanocomposites, pp 193–271
23. Da H. M. da Costa, R. C. R. Nunes, L. L. Y. Visconte, C. R. G. Furtado (2001) Kautschuk Gummi Kunststoffe 54: 5 242-249
24. Markovic GS, Marinovic-Cincovic MT, Jovanovic V, Samarzija-Jovanovic S, Budinski-Simendic J, Natural rubber materials: blends and IPNs (Chap. 1). Composites and nanocomposites, vol 1, pp 1–27
25. Markovic GS, Marinovic-Cincovic MT, Jovanovic V, Samarzija-Jovanovic S, Budinski-Simendic J, Composites and nanocomposites, pp 181–204
26. Janos M, Bela P (2008) J Ind Eng Chem 14:535–563
27. Das A, Stockelhuber KW, Jurk R, Saphiannikova M, Fritzsche J, Lorenz H et al (2008) Polymer 49:5276–5283
28. Ahankaria SS, Kamal KK (2008) Mater Sci Eng A 491:454–460
29. Fu SY, Xi-Qiao F, Bernd L, Yiu-Wing M (2008) Compos B 39:933–961
30. Leblanc JL (2002) Prog Polym Sci 27:627–687
31. Marković G, Marinović-Cincović M, Valentova H, Ilavsky M, Radovanović B, Budinski-Simendić (2005) Mater Sci Forum 494:475–481
32. Janowska G, Rybinski P (2004) J Therm Anal Calorim 78:839–847
33. Grauic N (1967) Encyclopedia of polymer science and technology, vol 4. Wiley, New York, p 159
34. Tarrıo-Saavedra J, Lopez-Beceiro J, Naya S, Artiaga R (2008) Polym Degrad Stab 93:2133–2137
35. Tanrattanakul V, Udomkichdecha W (2001) J Appl Polym Sci 82:650
36. López-Manchado MA, Valentín JL, Carretero J, Barroso F, Arroyo M (2007) Eur Polym J 43:4143–4150
37. Rattanasom N, Saowapark T, Deeprasertkul C (2007) Polym Testing 26:369–377
38. Chakraborthy SK, Setua DK, De SK (1982) Rubber Chem Technol 55:1286
39. Setua DK, De SK (1984) J Mater Sci 19:983–988
40. Coran AY, Hamed P, Goettler LA (1976) Rubber Chem Technol 49:1167–1181
41. Chakraborthy SK, Setua DK, De SK (1982) Rubber Chem Technol 55:1286
42. Arumugam N, Tamareselvy K, Venkata RK (1989) J Appl Polym Sci 37:2645–2659
43. Ding R, Leonov AI (1966) J Appl Polym Sci 61(3):455–463
44. Poh BT, Wong KW (1998) J Appl Polym Sci 69(7):1301–1305
45. de León R, Morales G, Acuña P, Soriano F (2010) Polym Eng Sci 50(2):373–383
46. Choi SS (2000) J Appl Polym Sci 75(11):1378–1384
47. Marković G, Marinović-Cincović M, Radovanović B, Budinski-Simendić J (2007) Chem Ind Chem Eng Q 13(4):186–191
48. Radovanović B, Marković G, Radovanović A (2008) Polym Compos 29:692–697
49. Ray S, Das CK (2001) Polym Plast Technol Eng 40

50. Zanzing DJ (1993) Rubber Chem Technol 66:456
51. Baker CSL (1974) Rubber Chem Technol 5:5
52. Patra PK, Das CK (1998) J Appl Polym Sci 68:597
53. Lewan MV (1998) Blends of natural rubber. Champman & Hall, London, p 52
54. Poh BT, Wong KW (1998) J Appl Polym Sci 69:1301
55. Bridson JA (1978) Rubber chemistry. Applied Science Publishers, London, p 83
56. Lewan MV (1998) Blends of natural rubber. Champman & Hall, London, p 52